Edinburgh Research Explorer

Cross-Species Single-Cell Analysis Reveals Divergence of the Primate Microglia Program

1 **Cross-species analysis across 450 million years of evolution reveals conservation and**
2 **divergence of the microglia program**
3

4 Laufey Geirsdottir[1][†], Eyal David[1][†], Hadas Keren-Shaul[1][†], Assaf Weiner[1], Stefan Cornelius Bohlen[2], Jana
5 Neuber[2], Adam Balic[3], Fadi Sheban[1], Charles-Antoine Dutertre[4,5], Christine Pfeifle[5], Francesca Peri[6],
6 Antonella Raffo-Romero[7], Jacopo Vizioli[7], Kaspar Matiasek[8], Christian Scheiwe[9], Stephan Meckel[10],
7 Kerstin Mätz-Rensing[15], Franziska van der Meer[15], Finnbogi Rutur Thormodsson[18], Christine
8 Stadelmann[19], Noga Zilkha[20], Tali Kimchi[20], Florent Ginhoux[4,16,17], Igor Ulitsky[11], Daniel Erny[2,12][†], Ido
9 Amit[1,†,**] and Marco Prinz[2,13,14†]
10

11 **1** Department of Immunology, Weizmann Institute of Science, Rehovot 7610001, Israel. **2** Institute of Neuropathology, Faculty
12 of Medicine, University of Freiburg, Freiburg, Germany. **3** The Roslin Institute and Royal (Dick) School of Veterinary Studies,
13 University of Edinburgh, Easter Bush, EH25 9RG, United Kingdom. **4** Singapore Immunology Network (SIgN), A∗STAR. **5**
14 Program in Emerging Infectious Disease, Duke-NUS Medical School, 8 College Road, Singapore 169857, Singapore**. 6**
15 Developmental Biology Unit, European Molecular Biology Laboratory (EMBL), Meyerhofstrasse 1, 69117 Heidelberg,
16 Germany. **7** Univ. Lille, Inserm, U-1192—Laboratoire Protéomique, Réponse Inflammatoire et Spectrométrie de Masse-
17 PRISM, F-59000 Lille, France**. 8** Ludwig-Maximilians-University Munich Institute for Animal Pathology Veterinärstr. 13. D-
18 80539 Munich. **9** Clinic for Neurosurgery, Faculty of Medicine, University of Freiburg, Freiburg, Germany**. 10** Department of
19 Neuroradiology, Faculty of Medicine, Medical Center-University of Freiburg, University of Freiburg, Freiburg, Germany. **11**
20 Department of Biological Regulation, Weizmann Institute of Science, Rehovot 7610001, Israel. **12** Berta-Ottenstein-
21 Programme, Faculty of Medicine, University of Freiburg, Freiburg, Germany. **13** Signaling Research Centres BIOSS and
22 CIBSS, University of Freiburg, Freiburg, Germany. **14** Center for NeuroModulation, Faculty of Medicine, University of
23 Freiburg, Freiburg, Germany. **15** German Primate Center, Leibniz Institute for Primate Research, Göttingen, Germany**. 16**
24 Shanghai Institute of Immunology, Shanghai JiaoTong University School of Medicine, 280 South Chongqing Road, Shanghai
25 200025, China**. 17** Translational Immunology Institute, Singhealth/Duke-NUS Academic Medical Centre, the Academia, 20
26 college road, Discovery tower level 8, Singapore 169856, Singapore **18** Innovation Center Iceland, Reykjavik, Iceland **19**
27 Institute of Neuropathology, University Medical Center Göttingen, Göttingen, Germany **20** Department of Neurobiology,
28 Weizmann Institute of Science, Rehovot 76100, Israel.
29
30
31 † equally contributing first authors; † equal and co-corresponding authors; Lead contact: **
32 Correspondance : DE: daniel.erny@uniklinik-freiburg.de; IA: ido.amit@weizmann.ac.il; MP: marco.prinz@uniklinik-freiburg.de
33

34 **SUMMARY**
35

36 Microglia, the brain-resident immune cells, are critically involved in many physiological and
37 pathological processes, including neurodegeneration. Here we characterize microglia
38 morphology and transcriptional program across ten species spanning more than 450 million
39 years of evolution. We find that microglia express a conserved core gene program of
40 orthologous genes from rodents to human, including ligands and receptors associated with
41 interactions between glia and neurons. In most species, microglia show a single dominant
42 transcriptional state, while human microglia display significant heterogeneity. In addition, we
43 observed notable differences in several gene modules of rodents as compared to primate
44 microglia; including complement, phagocytic and susceptibility genes to neurodegeneration,
45 such as Alzheimer's and Parkinson's disease. Our study provides an essential resource of
46 conserved and divergent microglia pathways across evolution with important implications for
47 future development of microglia-based therapies in humans.

INTRODUCTION

Microglia are the primary resident immune cells of the central nervous system (CNS) parenchyma and are seeded during development from mesodermal progenitors (Alliot et al., 1999; Ginhoux et al., 2010; Kierdorf et al., 2013; Perdiguero et al., 2014). Lineage tracing studies using mice have demonstrated that they can persist in the brain through local self-renewal, with no significant replenishment of monocytes during homeostatic conditions (Ajami et al., 2011; Askew et al., 2017; Hashimoto et al., 2013; Tay et al., 2018; Yona et al., 2013). They can rapidly repopulate their niche by self-renewal if depleted (Bruttger et al., 2015; Najafi et al., 2018), showing their unique adaptation to the brain parenchyma. This brain-specific tissue environment induces functional specialization of microglia resulting in a highly distinct phenotype separate from other tissue macrophage populations (Gosselin et al., 2014; Lavin et al., 2014). Additionally, microglia have been shown to be susceptible to environmental stimuli, such as microbiome and neonatal infections (Erny et al., 215; Thion et al., 2018).

Depending on the brain region, microglia are estimated to compose 5-20% of all brain cells, (Lawson et al., 1990; Perry, 1998). Microglia shape important brain processes such as neuronal pruning and development (Parkhurst et al., 2013; Schafer et al., 2012). Importantly, innate immune activation is considered to be of a critical pathophysiologic significance in most neurodegenerative diseases such as Alzheimer's disease (AD), suggesting microglia as central players in disease pathology (Matcovitch-Natan et al., 2016). Recently, we and others have demonstrated that microglia specific pathways, such as Trem2-Tyrobp and ApoE are critical determinants in AD and other neurodegenerative diseases (Jansen et al., 2019; Lambert et al., 2013; Keren-Shaul et al., 2017). Incidences of neurodegenerative disorders have steadily increased over the last decades in line with higher life expectancies of humans (Drew, 2018). Despite immense efforts over the past decades to find a cure for neurodegenerative disorders using transgenic animal models, large differences are observed in multiple characteristics of disease manifestation in human versus animal models. A better understanding of the conserved and divergent pathways of microglia may highlight the impact and limitation of commonly used animal models for neurodegeneration.

Large-scale sequencing of animal genomes has paved the way for characterization of genomic elements that are highly conserved across millions of years of evolution (La Manno et al., 2016; Suryamohan and Halfon, 2015). However, major challenges remain when applying this for

82   analysis of gene expression conservation across cell types. Standard antibody-based cell type

83   purification across species remains challenging, as epitope and antibody differences and

84   impurities of the cell population captured with these antibodies across different species

85   significantly restrict accurate cross-species analysis (Giladi and Amit, 2018). Potentially,

86   single-cell RNA-sequencing (scRNA-seq) can overcome these challenges, bypassing the need

87   for pure cell sorting strategies. Accordingly, scRNA-seq has been used to deconvolve immune

88   cell type heterogeneity by identifying novel distinct immune cell subsets in health and diseases

89   (Jaitin et al., 2014; Keren-Shaul et al., 2017; Papalexi and Satija, 2018; Paul et al., 2016; Jaitin

90   et al., 2019; Li et al., 2019), and provided new insights into the development and evolution of

91   cell types (La Manno et al., 2016; Pollen et al., 2015; 2014; Sebé-Pedrós et al., 2018; Treutlein

92   et al., 2014; Zeisel et al., 2015).

93

94   Here, we comprehensively characterize the conservation and divergence of the microglia

95   program across evolution. By comparing microglia gene expression across species, we identify

96   a conserved microglia core program in all mammals. Single cell analysis showed that most

97   mammalian microglia display one primary transcriptional state without any other apparent

98   subtypes. However, predominantly in humans, we observed substantial microglial

99   heterogeneity, with subtypes of microglia transcriptional signatures that are common to all

100   individuals examined. Importantly, microglia also contained species- and clade-specific gene

101   expression pathways associated with the complement system, phagocytosis and metabolic

102   pathways. By cross-comparing the microglia gene-expression with genome wide association

103   studies (GWAS) of human neurodegenerative diseases, we observed significant expression

104   changes of susceptibility genes for AD and Parkinson's disease (PD) in primates and humans

105   compared to rodents. In summary, we show the importance of cross evolutionary comparison

106   to better characterize human-specific microglia pathways and the relevance of these to human

107   disease. Our data offers an essential resource for the neuroimmunology community to move

108   forward towards the development of immunotherapy-based treatments for neurodegenerative

109   and neurodevelopmental disorders.

110

111   **RESULTS**
112

113   **Parenchymal microglia display a conserved morphological pattern across evolution**

114   To determine microglia conservation across evolution, we collected brain tissue of eighteen

115   evolutionary distant species for detailed microscopical analysis (**Figure 1A**). We identified

116   microglia using ionized calcium binding adaptor molecule 1 (Iba1), a prototypical marker for

117   microglia, perivascular macrophages, and monocytes of human, rats and, mice (Prinz and

118   Priller, 2014) that has been traditionally used to identify microglia within the parenchyma, as

119   other glial cells and neurons do not express it. Iba1 immunohistochemistry-based 3D-Imaris

120   analysis revealed that 16 of the 18 animals were positive for parenchymal Iba$^+$ cells, whereas

121   chicken and zebrafish were not (**Figure 1B**). The pan-myeloid markers mPEG1 (mPEG1-GFP

122   zebrafish) (Ellett et al., 2011) and CSF1R (CSF1R-mApple chickens) (Balic et al., 2014) were

123   subsequently used for myeloid identification within the parenchyma of these species (**Figure

124   1B**). Microscopic analysis of Iba1$^+$, mPEG$^+$ and CSF1R$^+$ parenchymal myeloid cells showed

125   cells with typical microglial morphology including, spindle-shaped soma and a distinct

126   arborization pattern as described before (Sierra et al., 2016) (**Figure 1B and S1A**). The

127   distinctive morphology and widespread distribution of these cells were highly consistent with

128   the classical descriptions of ramified microglia. These findings suggest that CNS parenchymal

129   cells with microglia-like features and markers can be found across all these animals, although

130   we observed a considerable range of ramification and cell sizes between species (**Figure 1B

131   and S1A**). Analysis of mouse and human microglial morphology revealed a partial region-

132   specific heterogeneity in both species, including smaller dendrite length, smaller number of

133   segments, and fewer branch points and terminal points in the molecular layer of the cerebellum

134   (**Figure S1B-C**). In general, the overall morphology of human microglia showed the highest

135   similarity to macaque, mouse, rat, hamster, sheep, boar, bat and chicken microglia in terms of

136   dendrite length, number of branching segments, terminal points and volume (**Figures 1B-G

137   and S1A**). The highest microglial density was detected in leech ganglia with 299.0 ± 41.4 Iba1$^+$

138   microglia per mm² and lowest microglial numbers in axolotl (11.1 ± 0.7 per mm²) (**Figures 1H-

139   I**).

140

141   We quantified the number of neurons in the cortex (**Figure 1J**) and neurons per microglia

142   (**Figure 1K**). In correlation analysis, we detected positive correlation of microglial density per

143   mm² and microglia process length across species (**Figure S1D**), whereas we did not observe

144   any detectable correlation between microglial and neuronal density (**Figure S1E**) or

145   microglia/neuron ratio and microglia process length (**Figure S1F**). In line with previous reports

146   (Menassa and Gomez-Nicola, 2018), we detected a higher microglial density in the frontal

147   cortex of mice (65.8 ±1.09 cells/mm^2) compared to human frontal cortex (35.5 ±2.48

148   cells/mm^2), and more microglia in the human cerebellum (molecular layer), hippocampus and

149   white matter compared to the respective regions in mice (**Figure S2A-D**). In summary,

150   histological analysis shows that microglial density varies markedly across the species even

151   among rodents and larger mammals. Further, while microglia display typical and conserved

152   morphology, the degree of ramification and cell size differs considerably in many of the species

153   examined.

154

155   **Characterization of the microglia gene expression program across species**

156   To better understand the divergence and conservation of the microglia gene expression across

157   evolution, we collected brains from three to six individuals for the eight species that had a high-

158   quality reference genome: human, macaque, marmoset, sheep, mouse, hamster, chicken and

159   zebrafish. Since even carefully sorted samples for bulk RNA-seq contain contaminating cells,

160   and scRNA-seq may potentially not be sensitive enough for detection of lowly expressed genes,

161   we used a combined single cell and bulk RNA-seq strategy to characterize the microglia gene

162   program across evolution (**Figure 2A**; **STAR Methods**). Analysis of the single cell data was

163   then used to deconvolute the bulk RNA-seq data and remove contaminating genes (**Figure 2A**;

164   **STAR Methods**) (Baron et al., 2016).

165

166   In order to preserve the *in situ* transcriptional state of microglia, all samples were freshly

167   processed and FACS sorted using a highly conserved pan immune marker; Protein tyrosine

168   phosphatase, receptor type C (Ptprc/ CD45; **Figure S3A**) (Holmes, 2006; Nagata et al., 2002;

169   Okumura et al., 1996). Cells were sorted for massively parallel single-cell RNA sequencing

170   (MARS-seq2.0) analysis (Jaitin et al., 2014; Keren-Shaul et al., 2019) or for bulk RNA

171   sequencing (**Figure 2A**). We collected a total of 4458 quality controlled (QC) -positive

172   microglia cells from eight species as well as three to six bulk RNA-seq samples for each species

173   (**Figure S3B-D** and **Table S1**). The Metacell algorithm (Baran et al., 2018; Giladi et al., 2018)

174   was used to identify homogeneous and robust groups of cells ("Metacells"; **STAR Methods**).

175   The majority of immune cells in the examined species were identified as microglia based on

176   their gene signature. Nonetheless, most species contained some metacells that were identified

177   as contaminating cells **(Table S1)**. For example, in chicken, analysis of CD45$^+$ brain cells

178   revealed two major groups of immune populations (**Figure 2B**). The first group expressed the

179   microglia gene signature, including multiple typical microglia markers that have already been

180   identified in human and mice microglia (e.g., *SALL1, P2RY12, C1QB*; **Figure 2B**), while the

181   second group expressed marker genes associated with T cells (e.g. *CD3E, RORA* and *IL7R*)

182   (**Figure 2B**). In order to focus on the microglia cells, after identification of contaminating cell

183   clusters, we removed the genes associated with these clusters from the bulk RNA-seq data

184   (**Figure 2C-D, S3E; STAR Methods**). We applied this method of microglia single cell

185   characterization and bulk RNA-seq deconvolution data analysis to all species. Together, these

186   findings highlight the potential of scRNA-seq to define with minimal biases conserved cell type

187   transcriptional signature across species, enabling a marker-free molecular comparison of the

188   microglia program across evolution.

189

190   **Microglia express a core gene program across evolutionary distant species**

191   To compare gene expression across species, we first defined a set of homologous genes across

192   species. We used a "meta-gene" strategy to solve the one-to-many and many-to-many

193   relationships of orthologues that have changed in evolution through duplication/deletion events

194   (**STAR Methods**). Orthologue conjecture is widely accepted as a method to pair genes over

195   evolution as orthologues diverge slowly, most explicitly in a tissue-specific manner, whereas

196   paralogs do not (Kryuchkova-Mostacci and Robinson-Rechavi, 2016). After filtering for lowly

197   expressed genes, we identified 8890 genes that were expressed in microglia of at least one of

198   the species (**STAR Methods**). Gene quantile normalization, followed by clustering analysis of

199   the deconvoluted bulk and scRNA-seq of microglia across evolution, identified 17 prominent

200   gene clusters (**Figure 3A and S4A; STAR Methods**). These clusters include a microglia core

201   signature expressed in all species (Clusters 1-10), but to a lesser extent in the zebrafish and

202   chicken, as well as clade and species-specific programs (Clusters 11-17; **Figure 3A** and **S4A**).

203   Hierarchical clustering across samples grouped the species based on their evolutionary distance

204   and displayed two major groups with the zebrafish and chicken microglia forming an outgroup

205   from the mammals (**Figure 3A**). This was not affected by the number of clusters or analysis

206   method and similar results were seen when applying principal component analysis (PCA;

207   **Figure S4B).** Macaque showed the highest similarity in expression patterns to human microglia

208   while laboratory mouse strains clustered together with wild mice and hamster (**Figure 3A** and

209   **Figure S4A-E**, **Table S3; STAR Methods**).

210

211   The transcription factors *Spi1* and *Irf8* have been shown to be the core orchestrators for

212   microglia development (Hoeffel et al., 2015; Kierdorf et al., 2013). *Tgfb2r* and *Csf1r* have also

been demonstrated to play an essential signaling role in microglia development, where the absence of these genes or inhibition of their signaling shows marked reduction or complete absence of microglia (Butovsky et al., 2014; Cronk et al., 2018; Elmore et al., 2014; Matcovitch-Natan et al., 2016; Pridans et al., 2018). *CSF1R* mutations also reduce microglia numbers in the human brain (Colonna and Butovsky, 2017). Consistent with these results, we observed strong conservation and expression of *Spi1*, *Irf8*, *Csf1r*, and *Tgfb2r* across all species, supporting the idea of the central role of these factors in microglia biology (**Figure 3A-B, and S4C**). Lysosomal hydrolases (e.g. *Cst3, Ctsa, Ctss, Ctsb, Ctsh, Ctsc, Ctsz,* and *Hexa*) were observed to be both highly expressed and conserved across mammalian species. Several of them are ubiquitously expressed in macrophages (e.g. *Ctsb, Ctsh, Ctsc*), but others have more restricted tissue expression, and their absence (e.g. *Ctsa* and *Hexa*) can cause severe neurological phenotypes (Caciotti et al., 2013). Another highly expressed and conserved lysosomal gene *Grn* (or progranulin), has been implicated in frontotemporal dementia in humans and mice (Baker et al., 2006).

Microglia genes that have been previously linked to the homeostatic gene signature of microglia are both highly expressed and conserved in all species, including *C1qc, P2ry12* and *Tardbp* (**Figure 3B-C** and **S4C**). *Tardbp* was recently shown to be protective against synapse loss in an AD mouse model, whereas its absence promoted higher amyloid clearance by enhancing phagocytosis (Paolicelli et al., 2017). *Vsir* (or VISTA) is an immune checkpoint gene, which inhibits T-cell response (Xu et al., 2018) and is highly conserved in all microglia (**Figure 3C** and **S4C**). Its expression has been shown to be increased in several neurological diseases, such as AD (Borggrewe et al., 2018). Interestingly, previously identified markers for yolk-sac derived microglia (e.g., *Daglb, Bin1, Cst3, Sall1, Prpsap2, Entpd1, Tmem119, P2ry12,* and *CD81*; **Figure 3B-C** and **S4C**) were present in core microglia clusters 1-3. These genes are highly enriched in microglia, and are not upregulated in monocytes that engraft the brain in microglial-depleted mouse models (Bennett et al., 2018; Cronk et al., 2018; Shemer et al., 2018).

Many of the conserved microglia genes in clusters 1-3 are shared by other tissue macrophages, which underlines the sentient role of the microglia/macrophage as phagocytic and defense cells in multicellular organisms (**Figure S4F** and **Table S4**). In order to identify the conserved microglia specific genes, we next compared our cross-species core signature (Clusters 1-3) to previously published datasets of a large compendium of mouse tissue-macrophages (Lavin et

247   al., 2014). This was done with the aim to discover highly conserved and cross-species genes

248   specific for microglia but not to other tissue macrophages (Lavin et al., 2014). Our cross-species

249   analysis identified 163 genes that are both conserved and unique to microglia (**Figure 3D** and

250   **Table S4;** Lavin et al., 2014). Among them is *Adgrg1* (*Gpr56*), previously demonstrated to be

251   conserved in human, mouse, and zebrafish, but also implicated in the development of

252   oligodendrocytes (Giera et al., 2018). Another conserved microglial gene is amyloid β

253   precursor protein-binding family b member 1 interacting protein (*Apbb1ip*) (**Figure 3D**), a

254   binding partner of the amyloid precursor protein (APP), Tau, 14-3-3γ, and glycogen synthase

255   kinase 3 β (GSK3 β). We further identified brain-specific functions, for example regulation of

256   neuron projection development and cerebellum development, as the most enriched gene

257   ontology pathways associated with these microglial specific genes (**Figure S4G**). These results

258   indicate that microglia express a large set of conserved core genes across all mammalian

259   species, including genes relevant for general tissue macrophage functions as well as microglia

260   specific CNS adaptations. In addition, we could confirm two of those markers, P2RY12 and

261   PU.1 by histology in several animals (**Figure S5A** and **S5B**, respectively).

262

263   **Single-cell transcriptomic analysis identifies human microglia subsets**

264   In order to examine whether the microglia of each specie display a homogenous cell type or

265   contain several subtypes, we further analyzed the microglia single cell data to evaluate

266   microglia heterogeneity for each mammalian species. We first clustered microglia cells from

267   each species separately and compared the intra- *versus* inter-cluster correlation to evaluate

268   whether there is a clear separation of microglia sub-types or a continuum of a single population

269   (**Figure 4A**). Surprisingly, we observed low inter-cluster correlation in all human samples

270   compared to intra-clusters (**Figure 4A**). Cell-to-cell correlation analysis revealed that microglia

271   from all human individuals are organized into several microglia-types (**Figure 4B**), which

272   confirms previous reports (Masuda et al., 2019). This was in sharp contrast to mouse (**Figure**

273   **4C**), macaque (**Figure S6A**), marmoset (**Figure S6B**), hamster (Figure **S6C**), and sheep

274   (**Figure S6D**), which show high intra-cluster correlation and predominantly one dominant

275   microglia type. Probing the heterogeneity of human microglia, we observed a sub-population

276   with increased expression of several inflammatory genes that have been linked with a

277   senescence-associated secretory phenotype (SASP) (Kobbe, 2018) (**Figure 4D**), without any

278   change of homeostatic gene expression (**Figure 4D**). This inflammatory signature of potentially

279   senescent-like microglia has been identified in most tissues of all ages in human and mice but

280   their number increases with age (He and Sharpless 2017). These cells are implicated in sterile

inflammation, wound healing, and age-related processes, including neurodegeneration (Bussian et al., 2018). Further investigation of these putative senescent-like microglia revealed that they were not specific to a single individual, but were consistent across all six sampled individuals, comprising roughly 20% of all microglia (**Figures 4E**). This microglia subset consistently co-expressed *CDKN1*, *CCL3, CCL4, CCL3L3* and *CCL4L2* (**Figures 4F**) along with higher expression of inflammatory cytokines such as *TNF* and *IL1B* (**Figure 4B, 4D**). This signature was not observed in young-adult mouse microglia (**Figure 4C**), but inflammatory cytokines have been previously seen in a sub-set of microglia in aged C57Bl/6 mice (Hammond et al., 2019; Sierra et al., 2007; Mrdjen et al., 2017).

A potential source of human microglia heterogeneity may involve interaction with the non-sterile environment. However, we did not observe microglia heterogeneity in wild mice (**Figure S6E**). Laboratory mouse models have been described to show considerable differences regarding the immune system regulation (Sellers et al., 2012). However**,** the microglia expression program of all mouse strains showed high similarity to each-other (**Figure S6F**), and only a small number of genes were identified as differential between the mouse strains (**Figure S6G**) Furthermore, comparing non-challenged microglia from four laboratory mouse strains housed in a specific pathogen free (SPF) facility, with wild mice housed in a non-SPF facility (including pathogens that are present in a natural environment), revealed only few differences (**Figure S6H**). In summary, single-cell transcriptomic analysis identifies major microglia heterogeneity in humans, in contrast to other mammals that mostly display a single microglia type in steady state, under non-pathological conditions.

Interspecies comparison identifies divergence in metabolic and immune pathways

In order to better understand the conservation of genes associated with neurodegenerative diseases, we have expanded our transcriptome analysis to include additional commonly studied rodent models: the rat (*Rattus norvegicus*), and the long-lived blind mole rat (BMR, *Spalax ehrenbergi;* maximum life-span of 20.2 years) (**Figure S7A-B**). Pairwise comparison of human microglia scRNA-seq transcriptomic data to rodents, identified a large module of differentially expressed genes (**S7A-B** and **Table S5**). In contrast, we observed a considerably smaller number of differentially expressed genes between human and macaque microglia, with most of the differentially expressed genes related to metabolic pathways such as NAD kinase (*NADK*; soluble vitamins metabolism) and beta-carotene oxygenase 2 (*BCO2*; carotenoid oxidization) (**Figure 5A**).

315

Pathway analysis of clusters specific to humans, macaque, marmoset, and sheep compared to rodents revealed enrichment of DNA repair pathways (**Figure S7D**), which have been previously implicated in longevity (Ungavari et al., 2008). Additionally, enriched pathways included phagocytosis (**Figure S7E**), more specifically apoptotic cell clearance (**Figure S7F** and **Table S6**) and the complement pathway (**Star Methods**; **Figure S7G** and **Table S6**). Several other pathways were enriched in all tested mammals except mice, in particular negative regulation of the ferroptosis pathway (**Figure S7H**). Ferroptosis is a newly described form of cell death driven by loss of activity of the lipid repair enzyme glutathione peroxidase 4 (*GPX4*) and subsequent accumulation of lipid-based reactive oxygen species (ROS), along with cytosolic accumulation of iron. Interestingly, several of those cellular events, including defects in phagocytosis, are thought to be hallmark drivers of many neurodegenerative diseases, including AD and PD.

Conservation and divergence of microglia neurodegenerative related pathways

Rodent animal models are critical for our understanding of many physiological and disease mechanisms. However, successful translation from neurodegenerative animal models to human clinical trials is far from adequate (Doody, 2017; Sperling et al., 2014; Vellas et al., 2014). In order to better understand the conservation of microglia genes associated with neurodegenerative diseases, we compared human microglia to commonly used animal models. We compared the gene expression of neurodegenerative disease susceptibility genes from GWAS studies of human microglia as compared to the other mammalian species (**STAR methods**; **Figure 5B**). Expression of Parkinson and Alzheimer's disease associated genes in human microglia showed highest correlation with macaque (PD, $r = 0.73$; AD, $r = 0.59$) (**Figure 5B**). In contrast, mice, rats and hamsters showed moderate to low correlation of AD and PD susceptibility genes to humans ($r = 0.16 - 0.40$) (**Figure 5B**). We observed significant over-representation for PD genes in the human specific cluster and clusters shared by human and macaques (**Figure S8A**). Conversely, we did not see any significant enrichment nor depletion of genes from GWAS studies of Schizophrenia or Huntington disease in any animal (**Figure 5B** and **S8C-D**). Human and macaque specific susceptibility genes included *Msr1* (macrophage scavenger receptor 1) (**Figure 5C and S8G**). *Msr1* mediates endocytosis of low density lipoproteins (LDL) and is involved in uptake and degradation of amyloid β (Aβ) (Frenkel et al., 2013). Previously, genes expressed by microglia have been implicated in AD in human genome-wide association studies (Gandal et al., 2018; Jansen et al., 2019; Keren-Shaul et al.,

349 2017). However, this is the first study identifying specific enrichment of AD and PD
350 susceptibility genes in microglia and their expression across evolution (**Figure S8A-B and E-**
351 **G**). In summary, our analysis identifies marked evolution in the expression of multiple
352 microglia pathways involved in metabolic, complement and phagocytic pathways, with many
353 of these pathways implicated in neurodegenerative diseases.
354
355 **DISCUSSION**
356
357 Effective development of therapies for neurodegenerative diseases is limited. This could be due
358 to the complexity of the CNS or potentially from lack of molecular understanding of relevant
359 animal models. In the current study, we systematically and comprehensively characterized
360 microglia from ten species of varying evolutionary distance, using a combination of single-cell
361 genomic technologies and histological analysis. We observed conservation of mammalian
362 microglia gene expression program, suggesting that microglia perform overall similar functions
363 throughout mammalian evolution. This is in accordance with previous reports showing high
364 constraints of brain gene expression-variance across evolution (Chan et al. 2009; Brawand et
365 al. 2011; Chen et al. 2019). Nevertheless, a substantial number of species-specific gene
366 expression was observed, which exhibited enrichment of several pathways that have not been
367 related to microglia or human microglia before. Our analysis of human, macaque and marmoset
368 revealed higher expression of pathways that have been implicated in longevity and anti-
369 inflammatory responses; more specifically - DNA repair pathways, negative regulation of
370 ferroptosis and apoptotic cell clearance. Many hallmarks of human neurodegeneration involve
371 specifically increased presence of double-strand DNA damage and senescent cells as well as
372 accumulation of iron and peroxidation of polyunsaturated fatty acids in CNS cells (Fielder et
373 al., 2017; Maynard et al., 2015; Sfera et al., 2018). These putative longevity pathways could
374 shed some light on the molecular basis of homeostatic microglial brain maintenance in long
375 living animals such as humans. Our analysis additionally revealed that human microglia express
376 the great majority of genes related to susceptibility to AD and PD (but not to Huntington or
377 Schizophrenia), whereas rodent microglia only express a fraction of these genes.
378
379 We identify substantial heterogeneity in human microglia as well as a sub-cluster of human
380 microglia that expressed a complex senescence-associated secretory phenotype (SASP), which
381 is thought to play a role in homing of immune cells for clearance of senescent cells (Lopes-
382 Paciencia et al., 2019). Regulation of SASP has been linked to several pathways, such as DNA

11

383 damage response and activation of immune response (Ito et al., 2017). As with any studies

384 involving human tissue, especially the CNS, caution has to be given to the interpretation of the

385 results. Although we exercised great care and carefully calibrated sample acquisition and

386 processing time (**STAR Methods**), it cannot be excluded that patients' microglia are not

387 accurately recapitulating the *in situ* states of healthy brains. Nonetheless, comparable studies

388 of human and mouse microglia with more extensive disease range (epilepsy, brain tumors, or

389 acute ischemia) showed very similar results (Gosselin et al., 2017; Masuda et al., 2019). This

390 supports our argument for human microglia heterogeneity that is not observed to this extent in

391 other species. In summary, our analysis identifies the microglia gene program across evolution.

392 It also provides a fundamental resource to compare microglia over a large evolutionary scale

393 and to guide future development and improvements in understanding of our laboratory models

394 of diseases mediated by microglia dysfunction.

395

396

421

422   AUTHOR CONTRIBUTIONS

430

431   DECLARATION OF INTEREST

432

433   The authors declare no competing interests.

FIGURE LEGENDS

435 **Figure 1. Quantitative analysis of microglia morphology in evolutionary distant animals.**

436 (**A**) Phylogenetic tree based on the NCBI taxonomy of animals used in this study (generated

437 via https://phylot.biobyte.de/). Ma = Million years. (**B**) Three-dimensional reconstruction (scale

438 bar represents 20 μm) and Imaris-based automatic quantification (**C-G**) of cell morphometry

439 of cortical Iba1$^+$, Mpeg1-eGFP$^+$ (zebrafish) and CSF1R-mApple$^+$ (chicken) microglia. Each

440 panel displays one individual sample with at least three measured cells per animal. Data are

441 presented as mean ± SEM. (**H**) Brain tissue was subjected to immunohistochemistry for Iba1

442 or stained with antibodies against the respective fluorescent proteins (zebrafish and chicken) to

443 detect microglia. Scale bar represents 50 μm. Representative images are displayed. (**I**) Number

444 of ramified parenchymal microglia in the CNS. (**J**) Number of cresyl violet$^+$ cortical neurons

445 in the CNS. (K) Calculated ratio of Neurons per microglia. For (H)-(K), each symbol displays

446 one individual sample. Three to four sections per sample were analyzed. Data is presented as

447 mean ± SEM.

448

449 **Figure 2. Transcriptional characterization of microglia across species.** (**A**) Illustrative

450 representation of RNA-seq strategy and cross-species characterization of microglia using flow

451 cytometry for single cell sort and bulk sort. Some of the examined species are shown as an

452 example. (**B**) Metacell analysis (of 629 cells and 22 Metacells) and heat-map representation of

453 30 differentially expressed genes and marker genes from CD45$^+$ single cell RNA-seq sorted

454 cells from a chicken brain. (**C**) Scatter (xy) plot showing the relationship of expressed genes

455 between all CD45$^+$ genes from combined single cell RNA-seq from chicken (x) and bulk RNA-

456 seq before *in silico* deconvolution (y). (**D**) Scatter (xy) plot showing the relationship of

457 expressed genes between bulk RNA-seq of chicken microglia before deconvolution (x) and

458 bulk RNA-seq of chicken microglia after deconvolution (y).

459

460 **Figure 3. Conserved microglia core gene expression program across evolution.** (**A**)

461 Heatmap representation of ranked bulk RNA-seq expression of *in silico* deconvoluted

462 microglia. Genes are clustered by the most differential gene expression (k-means=17) with

463 representative dendrogram showing nested groups of microglia genes measured by Pearson's

464 correlation coefficient. Annotations of shared and differential profile signature over species

465 considering top 50% (0.50 percentile) of all genes in the gene-set as a fixed expression threshold

466 (by row). Non- and lowly expressed genes are in the lowest percentile (0.5-0.67), medium

467 expressed genes in the mean percentile (0.68-0.85) and highest expressed genes in the top

468   percentile (0.86-1.0). Biological replicates; Human microglia (n=6), Marmoset microglia

469   (n=2), Macaque microglia (n=2), Hamster microglia (n=2), Sheep microglia (n=2), Chicken

470   (n=2), Zebrafish (n=2)**,** Mouse microglia (One individual from each strain depicted; C57Bl/6,

471   CD1, Balb/c, FVB, Wild mouse) (**B**) Bar plots of ranked bulk RNA-seq expression of highly

472   conserved and highly expressed genes identified in cluster 1 (as shown in A). Genes with no

473   orthologues are marked with a diagonally striped bar. (**C**) Violin-plots showing median (black

474   dot) and distribution of scRNA-seq gene expression (UMI count) across different replicates and

475   species. (**D**) Heatmap of mean gene expression of mouse microglia genes in cluster 1 to 3 (left

476   panel, highly conserved genes) compared to gene sets of mouse tissue macrophages as

477   described in (Lavin et al., 2014) (right panel). The most differentially expressed genes are

478   depicted (163 genes out of a total sum of 1791 genes from clusters 1-3).

479

480   **Figure 4. Identification of microglia heterogeneity using single cell RNA-seq analysis.** (**A**)

481   Scatter plot showing the relationship between inter- and intra-cluster correlation (Pearson

482   correlation r_s) of species. (**B-C**) Cell-to-cell correlation plot of microglia and corresponding

483   heatmap for most differentially expressed genes. In the heatmap, each mark represents one

484   metacell and each row marks the metacell from one individual. (**B**) Human microglia (n=6).

485   Color-barcoding marks each human individual at the bottom of the respective row. (**C**)

486   Microglia from wild mice (n=5). Color barcoding marks each mouse strain analyzed. (**D**)

487   Volcano plot showing the most differential genes between homeostatic microglia and microglia

488   subtypes (Metacells 3-6; p-value $< 10^{-7}$). Zoom in of specific genes for clarity is shown. (**E**)

489   Bar graph showing the contribution of each sample to corresponding gene expression (**F**) Gene-

490   gene correlation heatmap of senescent-like cluster in human microglia (Metacells 3-6). Red

491   shows high correlation and blue shows anti-correlation.

492

493   **Figure 5. Inter-species comparison of homeostatic microglia uncovers species differences.**

494   (**A**) Scatter plot showing inter-species microglia gene expression. Gene expression is calculated

495   as log (sum of UMI)/number of cells. The genes related to the non-homeostatic subtypes of

496   human microglia (From Figure 4) has been removed from the analysis. A subset of differentially

497   expressed genes and marker genes are highlighted in red. (**B**) Spearman correlation of single

498   cell RNA-seq expression (UMI count) of genes expressed in (from left to right); Alzheimer's

499   susceptibility genes (AD), Parkinson's susceptibility genes (PD), Huntington's disease (HD),

500   and Schizophrenia (SCZ). Species from top to bottom; Human vs Macaque, Human vs.

501   Marmoset, Human vs. Rat, Human vs. Mouse, Human vs. BMR, and Human vs. Hamster (**C**)

502   Violin-plots showing median (black dot) and distribution of single cell RNA-seq gene

503   expression (UMI count) across different replicates and species.

504

STAR METHODS

506

CONTACT FOR REAGENT AND RESOURCE SHARING
508 Further information and requests for reagents should be directed to and will be fulfilled by lead
509 author Ido Amit (ido.amit@weizmann.ac.il).

EXPERIMENTAL MODEL AND SUBJECT DETAILS

Experimental animals
512 All experimental procedures were either approved by a local ethical review committee and
513 conducted in accordance with personal and project licenses under the UK Animals (Scientific
514 Procedures) Act (1986) or performed in accordance with institutional animal welfare guidelines
515 and were approved by the government of Baden-Wurttemberg, Germany. Details of
516 experimental animals can be found in the Supplemental Information.

517

Sample processing
519 Mice, rats, BMR and hamsters were trans-cardially perfused with PBS before tissue extraction
520 whereas other animals were not perfused due to size limitations. Whole brains (zebrafish,
521 chicken, hamster, mice, marmoset and macaque), or specific parts of the brain (cortex and white
522 matter from sheep and human), were collected. Surrounding human brain tissues (access tissue)
523 that had to be removed in order to reach the respective putative epileptic focus from individuals
524 undergoing brain surgery for epilepsy were placed in ice-cold PBS immediately after resection.
525 Absence of pathology was confirmed by histological analysis in the respective area by a
526 neuropathologist. In addition, samples from adult patients that underwent brain autopsies were
527 included if tumor or inflammatory diseases were absent.

METHOD DETAILS

Sample processing for histology and FACS
530 Single-cell suspensions of tissues for all animals, were achieved using mechanical dissociation,
531 followed by density gradient separation; Pellet was mixed with 37% percoll (Cat. no. P1644,
532 Sigma) and centrifuged in 800G for 30 min at 4ºC. Supernatant was discarded and pellet was
533 taken further for antibody staining, as described below. Cell suspension was treated with 1:4000
534 diluted DAPI solution in 1xPBS to label dead cells. Before proceeding with antibody staining,
535 cells were pre-incubated with mouse or human Fc receptor blocking antibody (BD Biosciences,
536 Cat. 553141) for 20 minutes at 4°C. For antibody staining, cells were incubated with antibody
537 cocktail for 20 minutes at 4°C. For FACS staining and setups, cells were acquired on FACS
538 Canto, LSRII and LSR Fortessa systems (BD Biosciences) and analyzed with Flowjo software
539 (TreeStar).

540

541

Histology
543 Histology was performed as described recently (Erny et al., 2015). Brains were removed and
544 fixed in 4% buffered formalin. Then brain tissue was dehydrated and embedded in paraffin. 3
545 µm thin sections were stained with Iba1 (cat. no. 019-19741, Wako) for all species except leech-
546 specific Iba1 ((Drago et al., 2014) provided by J.V.), anti-GFP (cat. no. A11122, Invitrogen)

547   for zebrafish and anti-mCherry (cat. no. ab125096, Abcam) for chicken microglia. In addition,
548   brain tissue was stained for P2Y12 (cat. no. AS-55043, AnaSpec) or with anti-GFP (cat. no.
549   A11122, Invitrogen) for zebrafish as well for PU.1 (Cat. no. 2258S, Cell Signaling, zebrafish:
550   cat. no. ab209983, Abcam) At least 3–4 brain sections per sample were evaluated.
551
552   **Three-dimensional reconstruction of microglia.**
553   Reconstruction of microglial cells was performed as described before (Erny at al., 2015). 30-
554   µm parasagittal FFPE sections from adult brain tissue were stained with anti-Iba1 (cat. no. 019-
555   19741, Wako) for all species except leech-specific Iba1 ((Drago et al., 2014) provided by J.V.),
556   anti-GFP (cat. no. A11122, Invitrogen) for zebrafish and anti-mCherry (cat. no. ab125096,
557   Abcam) for chicken microglia for 48 h, respectively (dilution 1:500 at 4 °C), followed by Alexa
558   Fluor 568–conjugated secondary antibody (cat. no. A11011, Life technologies) staining, which
559   was added at a dilution of 1:500 overnight at 4 °C. Nuclei were counterstained with DAPI.
560   Imaging was performed on an Olympus Fluoview 1000 confocal laser scanning microscope
561   (Olympus) using a 20× 0.95 NA objective. Z stacks were done with 1.14-µm steps in z direction,
562     $1,024 \times 1,024$ pixel resolution were recorded and analyzed using IMARIS software (Bitplane).
563   At least three cortical cells were reconstructed per analyzed sample.
564
565   **Flowcytometry single cell sorting**
566   Cell populations were sorted with MoFlo Astrios (Beckman Coulter) Prior to sorting, all
567   samples were filtered through a 70-µm nylon mesh (Cat. no. 352350, Corning). Samples were
568   gated for $CD45^+$ after exclusion of doublets and dead cells. Isolated cells were single cell sorted
569   into 384-well cell capture plates containing 2 µl of lysis solution and barcoded poly(T) reverse-
570   transcription (RT) primers for single-cell RNA-seq (Keren-Shaul et al., 2019). Immediately
571   after sorting, each plate was spun down to ensure cell immersion into the lysis solution, snap
572   frozen on dry ice, and stored at –80°C until processed.
573
574   **Flowcytometry bulk cell sorting**
575   Cell populations were sorted with MoFlo Astrios (Beckman Coulter). Prior to sorting, all
576   samples were filtered through a 70-µm nylon mesh (Cat. no. 352350, Corning). Samples were
577   gated for $CD11b^+CD45^{lo}$ microglia population or GFP^+ cells for zebrafish or
578     $CD45^+CSF1RmApple^+$ cells for chicken, after exclusion of doublets. 10,000 cells were sorted
579   into a low-bind Eppendorf tube containing 40 µl of lysis binding buffer. Immediately after
580   sorting, tubes were spun down to ensure cell immersion into the lysis solution, snap frozen on
581   dry ice, and stored at –80°C until processed.
582
583   **AB table**

Name	Source	Catalogue #	Secondary
CD45-PE, non-human primate	Miltenyi Biotec	130-091-897	
Mouse anti-chicken Bu-1a/b	Bio-Rad	MCA5764	IgG1
Mouse anti-sheep CD45	Bio-Rad	MCA896GA	IgG1
Mouse anti-chicken CD45 APC	Southern Biotech	8270-11	
Mouse anti-pig CD45 FITC	Bio-Rad	MCA1222F	
Marmoset CD45 PE	BioLegend	250204	
Alexa Fluor 488	BioLegend	406416	Anti-IgG
Mouse anti-human CD45 PE	BioLegend	304058	
Anti-mouse CD11b	eBioscences	17-0112-83	
Mouse FcR blocking antibody	BD Biosciences	553141	
Hu FcR Binding blocker	eBiosciences	14-9161-73	
Anti-NHP CD45 PE	BD Biosciences	552833	

Anti-Rat CD45 PE	BD Biosciences	554888	
Goat polyclonal CD11b antibody	Abcam	Ab62817	Goat IgG
Donkey anti-Goat IgG (H+L) APC	R&D systems	F0108	Anti-goat IgG

584

Massively Parallel Single-Cell RNA-seq Library preparation (MARS-seq2.0)
585
Single-cell libraries were prepared as previously described (Keren-Shaul, Nature Protocols,
586
2019). In brief, mRNA from cell sorted into cell capture plates are barcoded and converted into
587
cDNA and pooled using an automated pipeline. The pooled sample is then linearly amplified
588
by T7 in vitro transcription, and the resulting RNA is fragmented and converted into a
589
sequencing-ready library by tagging the samples with pool barcodes and Illumina sequences
590
during ligation, RT, and PCR. Each pool of cells was tested for library quality and concentration
591
is assessed as described earlier (Keren-Shaul, Nature Protocols, 2019).
592

593

Bulk RNA-seq library preparation
594
10,000 cells from each population were sorted into 40 µl of lysis/binding buffer (Invitrogen).
595
mRNA was captured with 12 µl of Dynabeads oligo(dT) (Invitrogen), washed, and eluted at
596
85°C with 10 µl of 10 mM Tris-Cl (pH 7.5). We used a derivation of MARS-seq as described
597
(Keren-Shaul, Nature Protocols, 2019), developed for single-cell RNA-seq to produce
598
expression libraries with a minimum of three replicates per population.
599

600

Genomes
601

	Species	Built	Ensemble
Human	*Homo sapiens*	hg38	ensemble v95
Mouse	*Mus musculus*	mm10	ensemble v95
Chicken	*Gallus gallus*	galGal5	ensemble v90
Marmoset	*Callithrix jacchus*	calJac3	ensemble v90
Macaque	*Macaca fascicularis*	Mmul 8.0.1	ensemble v90
Sheep	*Ovis aries*	Oar v3.1	ensemble v90
Zebrafish	*Danio rerio*	danRer10	ensemble v90
Hamster	*Mesocricetus auratus*	MesAur1.0	ensemble v90
Rat	*Rattus norvegicus*	Rnor 6.0	ensemble v95
Blind Mole Rat	*Nannospalax galili*	S.galili v1.0	ensemble v96

602

Bulk low-level processing and filtering
603
Mapping of reads was done using HISAT (version 0.1.6) (Kim et al., 2015). UMIs were filtered
604
if two reads with matching UMIs were mapped to the same genome position (<3kb distance).
605
Reads were associated with genes if they were mapped to an exon in the correct orientation of
606
the gene. Gene expression tables were created using analyzeRepeats.pl script from the HOMER
607
package (v4.8) giving the specie specific GTF file (-gff flag) and genome from ensembl as
608
input. (http://homer.ucsd.edu/homer/)
609

610

Ortholog gene selection
611
To compare between species, we first created a gene ortholog table using the mouse genome as
612
the reference gene list. We performed gene homology search, using ensemble multiple species
613
comparison tool (http://www.ensembl.org/biomart/martview). Briefly, each specie was
614
compared to mouse and high-quality orthologues genes list was extracted (gene order
615
conservation score above 75, whole genome alignment score above 75 and minimum sequence
616
identity above 80%). To account for gene paralogues and gene-duplication events, an
617
aggregated table of "meta-genes" was created. Each meta-gene may include all gene symbols
618
homologous to one mouse gene. For each organism, read counts were aggregated across all
619

620 manifestations of each meta-gene. (For example, if zebrafish's actb1 had 2 read, and actb2 3
621 read, the Actb meta-gene received 5 total reads). Missing genes in species were given NaN
622 value.
623
Deconvolution of bulk data by detecting single cell outliers
625 Bulk RNA-seq data can contain combination of cell types due to sample acquisition impurity
626 and existence of outlier cells. Single-cell data was used to clean up bulk samples in the
627 following approach: Single-cell data from each organism was clustered using the Metacell
628 package (Baran et al., 2018). Clusters were manually annotated as microglia or outlier cell
629 types, based on expression of core genes shared by all species. Each bulk sample can be
630 described as a linear combination of all the cell types included in the samples. Using
631 optimization algorithms, "L-BFGS-B" in R general-purpose function "optim", we computed
632 the contribution of contaminating Metacells. Then, we deconvoluted each bulk sample by
633 subtracting the relative contribution of the outlier clusters.
634
Bulk normalization
636 Comparing RNA-seq data between species is challenging as the total number of genes differ,
637 there are large differences in total read number, housekeeping genes expression profile changed
638 across evolution and many other factors effects conventual RNA-seq normalization methods.
639 To overcome this technical challenge, we decided to use gene-rank score instead of actual read
640 count (such as TPM/RPKM). All values in all species were ranked, based on their expression
641 value position, this ranked vector was used as transcription profile for all downstream analysis.
642 To discard lowly expressed genes, rank levels were floored to 0.5. Only genes with at least one
643 entry ranked higher than 0.8 were included in later. Overall, ~9k genes were used for clustering
644 (Figure 3A).
645
Bulk clustering
647 Ranked bulk RNA-seq data was cluster using the K-means algorithm (Matlab R2018a function
648 kmeans). The value of k was chosen by assessing the mean silhouette values (a measure of how
649 close each point in one cluster is to points in the neighboring clusters) for various k parameters
650 and selecting k that maximizes the average silhouette.
651
Single cells low-level processing and filtering
653 All RNA-Seq libraries were sequenced using Illumina NextSeq 500 at a median sequencing
654 depth of: human 39032, mouse 47777, zebrafish 31764, chicken 63187, marmoset 57111,
655 macaque 43212, sheep 47170, hamster 55582, rat 18633, Blind mole rat 11679 reads per single
656 cell. Detailed statistics in cell resolution on barcodes, reads, mapping and genes see **Table S1**.
657 Sequences were mapped to appropriate genome, demultiplexed, and filtered as previously
658 described (Jaitin et al., 2014), extracting a set of unique molecular identifiers (UMI) that define
659 distinct transcripts in single cells for further processing. We estimated the level of spurious
660 UMIs in the data using statistics on empty MARS-seq wells. Mapping of reads was done using
661 HISAT (version 0.1.6) (Kim et al., 2015); reads with multiple mapping positions were
662 excluded. Reads were associated with genes if they were mapped to an exon, using the
663 appropriate ensemble v90 reference genome. Exons of different genes that shared genomic
664 position on the same strand were considered a single gene with a concatenated gene symbol.
665 Cells with less than 500 UMIs were discarded from the analysis. All downstream analysis was
666 performed in R.
667
Single cells data processing and clustering

669 The Metacell pipeline (Giladi et al., 2018) was used to derive informative genes and compute
670 cell-to-cell similarity, to compute K-nn graph covers and derive a distribution of RNA in
671 cohesive groups of cells (or meta-cells), and to derive strongly separated clusters using
672 bootstrap analysis and computation of graph covers on resampled data. Default parameters were
673 used unless otherwise stated.

674

675 Clustering of cells was performed for FACS sorted cells. Cells with high (> 32) expression of
676 hemoglobin genes were discarded (HBB, HBA1, HBA2). UMI was filtered out of ERCC reads.
677 Mitochondrial genes and ribosomal genes were removed from the analysis. Cells with limit of
678 UMI count after all filtering was >500. We used bootstrapping to derive robust clustering (500
679 iterations; resampling 70% of the cells in each iteration, and clustering the co-cluster matrix
680 with minimal cluster size set to 20). No further filtering or cluster splitting was performed on
681 the meta-cells.

682

683 **Gene enrichment analysis**
684 We performed gene enrichment analysis of human specific cluster and the large mammals
685 cluster (cluster 11 and 12 of figure 3A clustering analysis) using the online Metascape
686 (http://metascape.org/) tool with default parameters, using all genes as background. Genes from
687 human senescent-like microglia cell cluster has been removed from the analysis. For gene
688 related to neurodegenerative diseases enrichment we used GWAS gene lists from the NHGRI-
689 EBI GWAS catalog (mapped to Genome Assembly GRCh38.p12 and dbSNP Build 151) and
690 perform hypergeometric distribution test for each cluster from figure 3A, $p<0.01$ was
691 considered significant.

692

693 **Single cells differential expression**
694 To compare single cell expression between species, UMI tables were transformed to meta-genes
695 as described above. For each organism, we used meta-cell clustering to discard outlier cells and
696 activated microglia. Each cell was normalized by cell size and log transformed. We tested for
697 significantly differential genes by FDR adjusted Wilcoxon test (p-value $< 10^{-10}$ and fold change
698 > 2).

699

700 **Bulk of Single cell**
701 Single cell UMI cells loaded as in Single cells differential expression test. All good cells UMI
702 was summed which resulted in a single column for each organism. The small table of single
703 column for each organism was normalized to same number of reads.

704

705 **Scatter plots**
706 Bulked single cell gene list was used. All genes from microglia core gene module (**Figure 3A**)
707 were plotted unless a gene was not existing in one of the two species.

708

709 **PCA**
710 PCA was done in (Matlab R2018a function PPCA) (Verbeek et al., 2002) based on sensible
711 principal components analysis.

712

713 **Defining a module gene signature**
714 To define a module gene signature for Metacells 3-6 of the human microglia (**Figure 4**), we
715 used the normalized UMI table to identify the most differential genes between our clusters and
716 identified a group of 26 genes (e.g. *Cdkn1*, *Ccl2, Tnf*) that exhibited a strong Pearson correlation
717 across the Metacells' log2 footprint expression of the 200 most variable genes excluding genes
718 associated with mitochondria and stress that were filtered from these lists in advance. The *p*-

719 value was calculated using Wilcoxon signed-rank test and false discovery rate (FDR)
720 correction. The threshold for differential genes was set at pValue < 1E-7.
721

DATA AND SOFTWARE AVAILABILITY

723 The accession number for the raw sequence reported in this paper is EGA: The accession
724 number for the processed data reported in this paper is NCBI GEO: GSE134707. Scripts
725 reproducing the analysis will be available at: https://bitbucket.org/amitlab/.

726

SUPPLEMENTARY FIGURE LEGENDS

728 **Figure S1. Related to Figure 1. (A)** Representative reconstructed ramified parenchymal
729 microglia cells and corresponding fluorescence images of Iba1$^+$, Mpeg1-eGFP$^+$ (zebrafish) and
730 CSF1R-mApple$^+$ (chicken) microglia (red) and DAPI (4′,6-diamidino-2-phenylindole, blue)
731 from all analyzed species. Scale bar represents 20 µm. **(B)** Three-dimensional reconstruction
732 (scale bar represents 10 µm) and Imaris-based automatic quantification (**C**) of cell
733 morphometry of cortical mouse and human Iba1$^+$ microglia from different brain regions (cortex,
734 cerebellum, hippocampus and white matter). Each symbol displays one individual sample with
735 at least three measured cells per animal. Data is presented as mean ± SEM Spearman correlation
736 analysis comparing (**C**) microglial per mm² and microglia process length, (**D**) microglia per
737 mm² and neurons per mm² and (**E**) microglia per 100 neurons ratio and microglia process
738 length.

739

740 **Figure S2. Related to Figure 1.** Quantitative assessment of mouse and human microglia and
741 neurons in different brain regions. Iba1$^+$ microglia and cresyl violet$^+$ neurons in the mouse and
742 human frontal cortex (**A**), cerebellum (**B**), hippocampus (**C**) and white matter (**D**) (left) and
743 quantification thereof (right). Scale bar represent 50 µm for Iba1 and 200, 100 or 50 µm for
744 cresyl violet. Each symbol displays one individual sample. Data is presented as mean ± SEM
745 Significant differences were determined by an unpaired *t*-test and marked with asterisks (****P**
746 **< 0.01, ***P < 0.001).**

747

748 **Figure S3. Related to Figure 2.** (**A**) Representative flow cytometric plots showing gating
749 strategy for brain CD45$^+$ single-cell RNA sequencing sort. (**B**) Total UMI/cell count per
750 plate/animal. (**C**) UMI/cell count after filtering for microglia. (**D**) Percentage of microglia
751 identified in each species from flow cytometry sorted brain CD45$^+$ single cells. (**E**) Scatter (xy)
752 plot showing the relationship of expressed genes between single cell RNA-seq of chicken

753 microglia based on Figure 2B cluster (x) and bulk RNA-seq of chicken microglia after
754 deconvolution (y).

755

756 **Figure S4. Related to Figure 3.** (**A**) Heatmap representation of an average of single-cell RNA-
757 seq expression (UMIs per cell/number of cells) of microglia across species (row). Clustering of
758 most differentiated genes (k=17). (**B**) Principal component analysis (PCA) plot of all genes
759 from all species and their biological replicates. (**C**) Bar plots of ranked bulk RNA-seq
760 expression of representative highly conserved and highly expressed genes identified from
761 clusters 1-3 (as shown in Fig. 3A). Error bars show standard deviation (SD). Genes with no
762 orthologues are marked with a diagonally striped bar. (**D-E**) Correlation of global expression
763 signature of microglia across species measured by Spearman rank correlation (r_s) (**D**) of single
764 cell RNA-seq from all species (**E**) of bulk RNA-seq of microglia of species. Significant
765 biological processes or pathways identified using Metascape software analysis of (**F**) all genes
766 from clusters 1-3 using all genes as a background or (**G**) microglia specific genes identified in
767 a comparative analysis of tissue macrophages and microglia in Fig. 3D, using all genes as a
768 background.

769

770 **Figure S5. Related to Figure 3.** (**A**) Representative P2Y12 immunohistochemistry
771 microscopical images from paraffin brain sections from human, macaque, marmoset, mouse,
772 sheep, boar or bat as well as representative immunofluorescence image from brain section from
773 zebrafish. Scale bar represents 100 µm or 25 µm (zebrafish). (**B**) Representative PU.1
774 immunohistochemistry microscopical images from paraffin brain sections from human,
775 macaque, marmoset, mouse, sheep or zebrafish. Scale bars represents 100 µm.

776

777 **Figure S6. Related to Figure 4.** (**A-F**) Cell-to-cell correlation plots of microglia and
778 corresponding heatmaps for most differentially expressed genes. In the heatmaps, each mark
779 represents one cell and each row the cells from one individual. (**A**) Marmoset microglia (*n*=5).
780 (**B**) Macaque microglia (*n*=5). (**C**) Hamster microglia (*n*=5). (**D**) Sheep microglia (*n*=5)
781 (**E**) Wild mouse microglia (*n*=5). (**F**) A tSNE plot showing five mouse strains: C57BL/6,
782 Balb/c, CD1, FVB and Wild mice (*n*=5, each strain). (**G**) A tSNE plot of the most differentiated
783 marker genes expressed in mouse strains. The intensity of color corresponds to increased
784 expression. (**H**) A x-y plot comparing bulk RNA-seq of wild mouse microglia with averaged
785 bulk RNA-seq expression of mouse strains in SPF conditions (C57BL/6, CD1, Balb/c, FVB).
786 The most significant genes (Wild vs. SPF averaged) are labeled.

788 **Figure S7. Related to Figure 5.** (**A-B**) Heatmap representation and clustering of most

789 differentiated genes (k=12) of (**A**) a deconvoluted bulk of microglia and (**B**) an average of

790 single-cell RNA-seq expression (UMIs per cell/number of cells) of microglia across species

791 (row). (**C**) x-y plots comparing bulked single cell RNA-seq of rodents to each other. Highest

792 differentially expressed genes are demonstrated. (**D**) Gene ontology (GO) terms enriched in

793 human, macaque, marmoset and sheep microglia (cluster 11; Figure 3A). Differential genes

794 from human senescent-like microglia has been removed from the analysis. (**E**) Gene ontology

795 (GO) terms enriched in homeostatic human microglia (cluster 8; **Figure S7A**). Differential

796 genes from human senescent-like microglia were removed from the analysis. (**F-H**) Heatmap

797 representations of Gene ontology (GO) terms enriched in clusters related to Figure S7A. Genes

798 from human senescent microglia cell cluster were removed from the analysis. Highest

799 significantly enriched pathways in homeostatic human microglia (cluster 8) are represented.

800 (**F**) Specific genes from the classical complement pathway (GO: 0006956). (**G**) Specific genes

801 from apoptotic cell clearance (GO: 0043277). (**H**) Specific genes from ferroptosis pathway

802 (GO: 0097). Grey boxes indicate non-orthologue.

803

804   **Figure S8. Related to Figure 5.** (**A-D**) Clusters identified from cross-species comparison of

805 microglia (from Figure 3A) and visual demonstration of enrichment of GWAS terms shown as

806 fold change per cluster. Hypergeometric test was used to calculate the statistical significance

807 of under- or over-representation of a module of genes in clusters. Significantly enriched GWAS

808 gene lists (p = 0.001) are marked with an asterisk (*). Human clusters are colored in pink;

809 mouse clusters are colored in light blue. (**E-F**) Heatmap of gene expression of specific

810 neurodegenerative diseases defined by published GWAS from the NHGRI-EBI GWAS catalog

811 (mapped to Genome Assembly GRCh38.p12 and dbSNP Build 151). Genes that are specifically

812 absent or lowly expressed in mouse but not in humans are demonstrated. Grey boxes indicate

813 there is no homologous gene. (G) Violin-plots of specific genes related to specific

814 neurodegenerative diseases defined by published GWAS as in panels E to F.

815

816 **SUPPLEMENTARY TABLE LEGENDS**

817 **Table S1. Sample information. Related to Figure 1-2**.

818 **Table S2. Differential gene expression analysis of cross-species comparison of ranked**

819 **expression values of microglia genes. Related to Figure 3**. First tab includes all animals while

820 the second tab includes only the mammalian orthologs.

821 **Table S3. Pearson correlation of deconvoluted bulk microglia. Related to Figure S4D.**
822 Pearson correlation of ranked gene expression values of microglia.
823 **Table S4. Comparison of highly conserved microglia genes to tissue macrophage genes.**
824 **Related to Figure 3 and Table S2.** Highly expressed and conserved microglia genes from
825 cluster 1-3 (Figure 3; Table S2) compared to gene sets of mouse tissue macrophages as
826 described in (Lavin et al., 2014). The most differentially expressed genes are depicted (163
827 genes out of a total sum of 1791 genes from clusters 1-3
828 **Table S5. Pairwise comparison of human vs. other mammals, related to Figure 5 and S7.**
829 Most differential genes between human and the most common mammalian animal models.
830 **Table S6. Pathway analysis of clusters related to Figure 3 and Table S2**. RNA-seq gene
831 expression of specific pathways defined by Gene ontology (GO) terms

REFERENCES

Ajami, B., Bennett, J.L., Krieger, C., McNagny, K.M., and Rossi, F.M.V. (2011). Infiltrating monocytes trigger EAE progression, but do not contribute to the resident microglia pool. Nature Publishing Group *14*, 1142–1149.

Alliot, F., Godin, I., and Pessac, B. (1999). Microglia derive from progenitors, originating from the yolk sac, and which proliferate in the brain. Brain Res. Dev. Brain Res. *117*, 145–152.

Askew, K., Li, K., Olmos-Alonso, A., Garcia-Moreno, F., Liang, Y., Richardson, P., Tipton, T., Chapman, M.A., Riecken, K., Beccari, S., et al. (2017). Coupled Proliferation and Apoptosis Maintain the Rapid Turnover of Microglia in the Adult Brain. Cell Rep *18*, 391–405.

Baker, M., Mackenzie, I.R., Pickering-Brown, S.M., Gass, J., Rademakers, R., Lindholm, C., Snowden, J., Adamson, J., Sadovnick, A.D., Rollinson, S., et al. (2006). Mutations in progranulin cause tau-negative frontotemporal dementia linked to chromosome 17. Nature *442*, 916–919.

Balic, A., Garcia-Morales, C., Vervelde, L., Gilhooley, H., Sherman, A., Garceau, V., Gutowska, M.W., Burt, D.W., Kaiser, P., Hume, D.A., et al. (2014). Visualisation of chicken macrophages using transgenic reporter genes: insights into the development of the avian macrophage lineage. Development *141*, 3255–3265.

Baran, Y., Sebé-Pedrós, A., Lubling, Y., Giladi, A., Chomsky, E., Meir, Z., Hoichman, M., Lifshitz, A., and Tanay, A. (2018). MetaCell: analysis of single cell RNA-seq data using k-NN graph partitions.

Baron, M., Veres, A., Wolock, S.L., Faust, A.L., Gaujoux, R., Vetere, A., Ryu, J.H., Wagner, B.K., Shen-Orr, S.S., Klein, A.M., et al. (2016). A Single-Cell Transcriptomic Map of the Human and Mouse Pancreas Reveals Inter- and Intra-cell Population Structure. Cell Systems *3*, 346–360.e4.

Bennett, F.C., Bennett, M.L., Yaqoob, F., Mulinyawe, S.B., Grant, G.A., Hayden Gephart, M., Plowey, E.D., and Barres, B.A. (2018). A Combination of Ontogeny and CNS Environment Establishes Microglial Identity. Neuron.

Borggrewe, M., Grit, C., Dunnen, Den, W.F.A., Burm, S.M., Bajramovic, J.J., Noelle, R.J., Eggen, B.J.L., and Laman, J.D. (2018). VISTA expression by microglia decreases during inflammation and is differentially regulated in CNS diseases. Glia *66*, 2645–2658.

Bruttger, J., Karram, K., Wörtge, S., Regen, T., Marini, F., Hoppmann, N., Klein, M., Blank, T., Yona, S., Wolf, Y., et al. (2015). Genetic Cell Ablation Reveals Clusters of Local Self-Renewing Microglia in the Mammalian Central Nervous System. Immunity *43*, 92–106.

Butovsky, O., Jedrychowski, M.P., Moore, C.S., Cialic, R., Lanser, A.J., Gabriely, G., Koeglsperger, T., Dake, B., Wu, P.M., Doykan, C.E., et al. (2014). Identification of a unique TGF-β-dependent molecular and functional signature in microglia. Nature Publishing Group *17*, 131–143.

25

871 Caciotti, A., Catarzi, S., Tonin, R., Lugli, L., Perez, C.R., Michelakakis, H., Mavridou, I.,
872 Donati, M.A., Guerrini, R., d'Azzo, A., et al. (2013). Galactosialidosis: review and analysis of
873 CTSA gene mutations. Orphanet J Rare Dis *8*, 114.

874 Chakrabarty, P., Li, A., Ladd, T.B., Strickland, M.R., Koller, E.J., Burgess, J.D., Funk, C.C.,
875 Cruz, P.E., Allen, M., Yaroshenko, M., et al. (2018). TLR5 decoy receptor as a novel anti-
876 amyloid therapeutic for Alzheimer's disease. J. Exp. Med. *215*, 2247–2264.

877 Colonna, M., and Butovsky, O. (2017). Microglia Function in the Central Nervous System
878 During Health and Neurodegeneration. Annu. Rev. Immunol. *35*, 441–468.

879 Cronk, J.C., Filiano, A.J., Louveau, A., Marin, I., Marsh, R., Ji, E., Goldman, D.H., Smirnov,
880 I., Geraci, N., Acton, S., et al. (2018). Peripherally derived macrophages can engraft the brain
881 independent of irradiation and maintain an identity distinct from microglia. J. Exp. Med. *215*,
882 1627–1647.

883 Doody, R. (2017). Developing Disease-Modifying Treatments in Alzheimer's Disease - A
884 Perspective from Roche and Genentech. J Prev Alzheimers Dis *4*, 264–272.

885 Drago, F., Sautière, P.-E., Le Marrec-Croq, F., Accorsi, A., Van Camp, C., Salzet, M.,
886 Lefebvre, C., and Vizioli, J. (2014). Microglia of medicinal leech (Hirudo medicinalis)
887 express a specific activation marker homologous to vertebrate ionized calcium-binding
888 adapter molecule 1 (Iba1/alias aif-1). Dev Neurobiol *74*, 987–1001.

889 Drew, L. (2018). An age-old story of dementia. Nature *559*, S2–S3.

890 Ellett, F., Pase, L., Hayman, J.W., Andrianopoulos, A., and Lieschke, G.J. (2011). mpeg1
891 promoter transgenes direct macrophage-lineage expression in zebrafish. Blood *117*, e49–e56.

892 Elmore, M.R.P., Najafi, A.R., Koike, M.A., Dagher, N.N., Spangenberg, E.E., Rice, R.A.,
893 Kitazawa, M., Matusow, B., Nguyen, H., West, B.L., et al. (2014). Colony-Stimulating Factor
894 1 Receptor Signaling Is Necessary for Microglia Viability, Unmasking a Microglia Progenitor
895 Cell in the Adult Brain. Neuron *82*, 380–397.

896 Erny, D., Hrabě de Angelis, A.L., Jaitin, D., Wieghofer, P., Staszewski, O., David, E., Keren-
897 Shaul, H., Mahlakoiv, T., Jakobshagen, K., Buch, T., et al. (2015). Host microbiota constantly
898 control maturation and function of microglia in the CNS. Nature Publishing Group *18*, 965–
899 977.

900 Fielder, E., Zglinicki, von, T., and Jurk, D. (2017). The DNA Damage Response in Neurons:
901 Die by Apoptosis or Survive in a Senescence-Like State? J. Alzheimers Dis. *60*, S107–S131.

902 Frenkel, D., Wilkinson, K., Zhao, L., Hickman, S.E., Means, T.K., Puckett, L., Farfara, D.,
903 Kingery, N.D., Weiner, H.L., and Khoury, El, J. (2013). Scara1 deficiency impairs clearance
904 of soluble amyloid-β by mononuclear phagocytes and accelerates Alzheimer's-like disease
905 progression. Nature Communications *4*, 2030.

906 Gandal, M.J., Haney, J.R., Parikshak, N.N., Leppa, V., Ramaswami, G., Hartl, C., Schork,
907 A.J., Appadurai, V., Buil, A., Werge, T.M., et al. (2018). Shared molecular neuropathology
908 across major psychiatric disorders parallels polygenic overlap. Science *359*, 693–697.

909 Giera, S., Luo, R., Ying, Y., Ackerman, S.D., Jeong, S.-J., Stoveken, H.M., Folts, C.J.,
910 Welsh, C.A., Tall, G.G., Stevens, B., et al. (2018). Microglial transglutaminase-2 drives
911 myelination and myelin repair via GPR56/ADGRG1 in oligodendrocyte precursor cells. Elife
912 *7*, 6122.

913 Giladi, A., and Amit, I. (2018). Single-Cell Genomics: A Stepping Stone for Future
914 Immunology Discoveries. Cell *172*, 14–21.

915 Giladi, A., Paul, F., Herzog, Y., Lubling, Y., Weiner, A., Yofe, I., Jaitin, D., Cabezas-
916 Wallscheid, N., Dress, R., Ginhoux, F., et al. (2018). Single-cell characterization of
917 haematopoietic progenitors and their trajectories in homeostasis and perturbed
918 haematopoiesis. Nat. Cell Biol. *20*, 836–846.

919 Ginhoux, F., Greter, M., Leboeuf, M., Nandi, S., See, P., Gokhan, Ş., Mehler, M.F., Conway,
920 S.J., Ng, L.G., Stanley, E.R., et al. (2010). Fate mapping analysis reveals that adult microglia
921 derive from primitive macrophages. Science *330*, 841–845.

922 Gosselin, D., Skola, D., Coufal, N.G., Holtman, I.R., Schlachetzki, J.C.M., Sajti, E., Jaeger,
923 B.N., O'Connor, C., Fitzpatrick, C., Pasillas, M.P., et al. (2017). An environment-dependent
924 transcriptional network specifies human microglia identity. Science *356*, 1248–1259.

925 Gosselin, D., Link, V.M., Romanoski, C.E., Fonseca, G.J., Eichenfield, D.Z., Spann, N.J.,
926 Stender, J.D., Chun, H.B., Garner, H., Geissmann, F., et al. (2014). Environment drives
927 selection and function of enhancers controlling tissue-specific macrophage identities. Cell
928 *159*, 1327–1340.

929 Hashimoto, D., Chow, A., Noizat, C., Teo, P., Beasley, M.B., Leboeuf, M., Becker, C.D.,
930 See, P., Price, J., Lucas, D., et al. (2013). Tissue-resident macrophages self-maintain locally
931 throughout adult life with minimal contribution from circulating monocytes. Immunity *38*,
932 792–804.

933 Hickman, S.E., Kingery, N.D., Ohsumi, T.K., Borowsky, M.L., Wang, L.-C., Means, T.K.,
934 and Khoury, El, J. (2013). The microglial sensome revealed by direct RNA sequencing.
935 Nature Publishing Group *16*, 1896–1905.

936 Hoeffel, G., Chen, J., Lavin, Y., Low, D., Almeida, F.F., See, P., Beaudin, A.E., Lum, J.,
937 Low, I., Forsberg, E.C., et al. (2015). C-Myb(+) erythro-myeloid progenitor-derived fetal
938 monocytes give rise to adult tissue-resident macrophages. Immunity *42*, 665–678.

939 Holmes, N. (2006). CD45: all is not yet crystal clear. Immunology *117*, 145–155.

940 Ito, Y., Hoare, M., and Narita, M. (2017). Spatial and Temporal Control of Senescence.
941 Trends Cell Biol. *27*, 820–832.

942 Jaitin, D.A., Kenigsberg, E., Keren-Shaul, H., Elefant, N., Paul, F., Zaretsky, I., Mildner, A.,
943 Cohen, N., Jung, S., Tanay, A., et al. (2014). Massively parallel single-cell RNA-seq for
944 marker-free decomposition of tissues into cell types. Science *343*, 776–779.

945 Jaitin, D.A., Adlung, L., Thaiss, C.A., Weiner, A., Li, B., Descamps, H., Lundgren, P.,
946 Bleriot, C., Liu, Z., Deczkowska, A., et al. (2019). Lipid-Associated Macrophages Control
947 Metabolic Homeostasis in a Trem2-Dependent Manner. Cell *178*, 686–698.e14.

948 Jansen, I.E., Savage, J.E., Watanabe, K., Bryois, J., Williams, D.M., Steinberg, S., Sealock, J.,
949 Karlsson, I.K., Hägg, S., Athanasiu, L., et al. (2019). Genome-wide meta-analysis identifies
950 new loci and functional pathways influencing Alzheimer's disease risk. Nat. Genet. *9*, 63.

951 Keren-Shaul, H., Spinrad, A., Weiner, A., Matcovitch-Natan, O., Dvir-Szternfeld, R., Ulland,
952 T.K., David, E., Baruch, K., Lara-Astaiso, D., Toth, B., et al. (2017). A Unique Microglia
953 Type Associated with Restricting Development of Alzheimer's Disease. Cell *169*, 1276–
954 1290.e17.

955 Kierdorf, K., Erny, D., Goldmann, T., Sander, V., Schulz, C., Perdiguero, E.G., Wieghofer,
956 P., Heinrich, A., Riemke, P., Hölscher, C., et al. (2013). Microglia emerge from
957 erythromyeloid precursors via Pu.1- and Irf8-dependent pathways. Nature Publishing Group
958 *16*, 273–280.

959 Kobbe, von, C. (2018). Cellular senescence: a view throughout organismal life. Cell. Mol.
960 Life Sci. *75*, 3553–3567.

961 Kryuchkova-Mostacci, N., and Robinson-Rechavi, M. (2016). Tissue-Specificity of Gene
962 Expression Diverges Slowly between Orthologs, and Rapidly between Paralogs. PLoS
963 Comput Biol *12*, e1005274.

964 La Manno, G., Gyllborg, D., Codeluppi, S., Nishimura, K., Salto, C., Zeisel, A., Borm, L.E.,
965 Stott, S.R.W., Toledo, E.M., Villaescusa, J.C., et al. (2016). Molecular Diversity of Midbrain
966 Development in Mouse, Human, and Stem Cells. Cell *167*, 566–580.e19.

967 Lambert, J.C., Ibrahim-Verbaas, C.A., Harold, D., Naj, A.C., Sims, R., Bellenguez, C.,
968 DeStafano, A.L., Bis, J.C., Beecham, G.W., Grenier-Boley, B., et al. (2013). Meta-analysis of
969 74,046 individuals identifies 11 new susceptibility loci for Alzheimer's disease. Nat. Genet.
970 *45*, 1452–1458.

971 Lavin, Y., Winter, D., Blecher-Gonen, R., David, E., Keren-Shaul, H., Merad, M., Jung, S.,
972 and Amit, I. (2014). Tissue-resident macrophage enhancer landscapes are shaped by the local
973 microenvironment. Cell *159*, 1312–1326.

974 Lawson, L.J., Perry, V.H., Dri, P., and Gordon, S. (1990). Heterogeneity in the distribution
975 and morphology of microglia in the normal adult mouse brain. Neuroscience *39*, 151–170.

976 Li, H., van der Leun, A.M., Yofe, I., Lubling, Y., Gelbard-Solodkin, D., van Akkooi, A.C.J.,
977 van den Braber, M., Rozeman, E.A., Haanen, J.B.A.G., Blank, C.U., et al. (2019).
978 Dysfunctional CD8 T Cells Form a Proliferative, Dynamically Regulated Compartment
979 within Human Melanoma. Cell *176*, 775–789.e18.

980 Lopes-Paciencia, S., Saint-Germain, E., Rowell, M.-C., Ruiz, A.F., Kalegari, P., and
981 Ferbeyre, G. (2019). The senescence-associated secretory phenotype and its regulation.
982 Cytokine *117*, 15–22.

983 Masuda, T., Sankowski, R., Staszewski, O., Böttcher, C., Amann, L., Scheiwe, C., Nessler,
984 S., Kunz, P., van Loo, G., Coenen, V.A., et al. (2019). Spatial and temporal heterogeneity of
985 mouse and human microglia at single-cell resolution. Nature *15*, 300–392.

986 Matcovitch-Natan, O., Winter, D.R., Giladi, A., Vargas Aguilar, S., Spinrad, A., Sarrazin, S.,
987 Ben-Yehuda, H., David, E., Zelada González, F., Perrin, P., et al. (2016). Microglia

988   development follows a stepwise program to regulate brain homeostasis. Science *353*,
989   aad8670–aad8670.

990   Maynard, S., Fang, E.F., Scheibye-Knudsen, M., Croteau, D.L., and Bohr, V.A. (2015). DNA
991   Damage, DNA Repair, Aging, and Neurodegeneration. Cold Spring Harb Perspect Med *5*,
992   a025130.

993   Menassa, D.A., and Gomez-Nicola, D. (2018). Microglial Dynamics During Human Brain
994   Development. Front Immunol *9*, 1014.

995   Nagata, T., Suzuki, T., Ohta, Y., Flajnik, M.F., and Kasahara, M. (2002). The leukocyte
996   common antigen (CD45) of the Pacific hagfish, Eptatretus stoutii: implications for the
997   primordial function of CD45. Immunogenetics *54*, 286–291.

998   Najafi, A.R., Crapser, J., Jiang, S., Ng, W., Mortazavi, A., West, B.L., and Green, K.N.
999   (2018). A limited capacity for microglial repopulation in the adult brain. Glia *66*, 2385–2396.

1000   Okumura, M., Matthews, R.J., Robb, B., Litman, G.W., Bork, P., and Thomas, M.L. (1996).
1001   Comparison of CD45 extracellular domain sequences from divergent vertebrate species
1002   suggests the conservation of three fibronectin type III domains. J.I. *157*, 1569–1575.

1003   Paolicelli, R.C., Jawaid, A., Henstridge, C.M., Valeri, A., Merlini, M., Robinson, J.L., Lee,
1004   E.B., Rose, J., Appel, S., Lee, V.M.-Y., et al. (2017). TDP-43 Depletion in Microglia
1005   Promotes Amyloid Clearance but Also Induces Synapse Loss. Neuron *95*, 297–308.e6.

1006   Papalexi, E., and Satija, R. (2018). Single-cell RNA sequencing to explore immune cell
1007   heterogeneity. Nat. Rev. Immunol. *18*, 35–45.

1008   Parkhurst, C.N., Yang, G., Ninan, I., Savas, J.N., Yates, J.R., Lafaille, J.J., Hempstead, B.L.,
1009   Littman, D.R., and Gan, W.-B. (2013). Microglia promote learning-dependent synapse
1010   formation through brain-derived neurotrophic factor. Cell *155*, 1596–1609.

1011   Paul, F., Arkin, Y., Giladi, A., Jaitin, D.A., Kenigsberg, E., Keren-Shaul, H., Winter, D.,
1012   Lara-Astiaso, D., Gury, M., Weiner, A., et al. (2016). Transcriptional Heterogeneity and
1013   Lineage Commitment in Myeloid Progenitors. Cell *164*, 325.

1014   Perdiguero, E.G., Klapproth, K., Schulz, C., Busch, K., Azzoni, E., Crozet, L., Garner, H.,
1015   Trouillet, C., de Bruijn, M.F., Geissmann, F., et al. (2014). Tissue-resident macrophages
1016   originate from yolk-sac-derived erythro-myeloid progenitors. Nature 1–17.

1017   Perry, V.H. (1998). A revised view of the central nervous system microenvironment and
1018   major histocompatibility complex class II antigen presentation. J. Neuroimmunol. *90*, 113–
1019   121.

1020   Pollen, A.A., Nowakowski, T.J., Chen, J., Retallack, H., Sandoval-Espinosa, C., Nicholas,
1021   C.R., Shuga, J., Liu, S.J., Oldham, M.C., Diaz, A., et al. (2015). Molecular identity of human
1022   outer radial glia during cortical development. Cell *163*, 55–67.

1023   Pollen, A.A., Nowakowski, T.J., Shuga, J., Wang, X., Leyrat, A.A., Lui, J.H., Li, N.,
1024   Szpankowski, L., Fowler, B., Chen, P., et al. (2014). Low-coverage single-cell mRNA
1025   sequencing reveals cellular heterogeneity and activated signaling pathways in developing
1026   cerebral cortex. Nat. Biotechnol. *32*, 1053–1058.

1027 Pridans, C., Raper, A., Davis, G.M., Alves, J., Sauter, K.A., Lefevre, L., Regan, T., Meek, S.,
1028 Sutherland, L., Thomson, A.J., et al. (2018). Pleiotropic Impacts of Macrophage and
1029 Microglial Deficiency on Development in Rats with Targeted Mutation of the Csf1r Locus. J.
1030 Immunol. *201*, 2683–2699.

1031 Prinz, M., and Priller, J. (2014). Microglia and brain macrophages in the molecular age: from
1032 origin to neuropsychiatric disease. Nat. Rev. Neurosci. *15*, 300–312.

1033 Schafer, D.P., Lehrman, E.K., Kautzman, A.G., Koyama, R., Mardinly, A.R., Yamasaki, R.,
1034 Ransohoff, R.M., Greenberg, M.E., Barres, B.A., and Stevens, B. (2012). Microglia sculpt
1035 postnatal neural circuits in an activity and complement-dependent manner. Neuron *74*, 691–
1036 705.

1037 Sebé-Pedrós, A., Saudemont, B., Chomsky, E., Plessier, F., Mailhé, M.-P., Renno, J., Loe-
1038 Mie, Y., Lifshitz, A., Mukamel, Z., Schmutz, S., et al. (2018). Cnidarian Cell Type Diversity
1039 and Regulation Revealed by Whole-Organism Single-Cell RNA-Seq. Cell *173*, 1520–
1040 1534.e1520.

1041 Sellers, R.S., Clifford, C.B., Treuting, P.M., and Brayton, C. (2012). Immunological
1042 Variation Between Inbred Laboratory Mouse Strains. Vet Pathol *49*, 32–43.

1043 Sfera, A., Bullock, K., Price, A., Inderias, L., and Osorio, C. (2018). Ferrosenescence: The
1044 iron age of neurodegeneration? Mech. Ageing Dev. *174*, 63–75.

1045 Shemer, A., Grozovski, J., Tay, T.L., Tao, J., Volaski, A., Süß, P., Ardura-Fabregat, A.,
1046 Gross-Vered, M., Kim, J.-S., David, E., et al. (2018). Engrafted parenchymal brain
1047 macrophages differ from microglia in transcriptome, chromatin landscape and response to
1048 challenge. Nature Communications *9*, 5206.

1049 Sierra, A., de Castro, F., Del Río-Hortega, J., Rafael Iglesias-Rozas, J., Garrosa, M., and
1050 Kettenmann, H. (2016). The "Big-Bang" for modern glial biology: Translation and comments
1051 on Pío del Río-Hortega 1919 series of papers on microglia. Glia *64*, 1801–1840.

1052 Sperling, R., Mormino, E., and Johnson, K. (2014). The evolution of preclinical Alzheimer's
1053 disease: implications for prevention trials. Neuron *84*, 608–622.

1054 Suryamohan, K., and Halfon, M.S. (2015). Identifying transcriptional cis-regulatory modules
1055 in animal genomes. Wiley Interdiscip Rev Dev Biol *4*, 59–84.

1056 Tay, T.L., Sagar, Dautzenberg, J., Grün, D., and Prinz, M. (2018). Unique microglia recovery
1057 population revealed by single-cell RNAseq following neurodegeneration. Acta Neuropathol
1058 Commun *6*, 87.

1059 Thion, M.S., Low, D., Silvin, A., Chen, J., Grisel, P., Schulte-Schrepping, J., Blecher, R.,
1060 Ulas, T., Squarzoni, P., Hoeffel, G., et al. (2018). Microbiome Influences Prenatal and Adult
1061 Microglia in a Sex-Specific Manner. Cell *172*, 500–516.e516.

1062 Treutlein, B., Brownfield, D.G., Wu, A.R., Neff, N.F., Mantalas, G.L., Espinoza, F.H., Desai,
1063 T.J., Krasnow, M.A., and Quake, S.R. (2014). Reconstructing lineage hierarchies of the distal
1064 lung epithelium using single-cell RNA-seq. Nature *509*, 371–375.

1065 Vellas, B., Sampaio, C., Bateman, R., Boxer, A., Carrillo, M.C., Cummings, J., Dubois, B.,
1066 Hampel, H., Katz, R., Khachaturian, Z., et al. (2014). EU./U.S. CTAD Task Force on
1067 Alzheimer's Trial Populations. J Prev Alzheimers Dis *1*, 110–116.

1068 Verbeek, J., Vlassis, N., and Krose, B. (2002). Procrustes analysis to coordinate mixtures of
1069 probabilistic principal component analyzers.

1070 Yona, S., Kim, K.-W., Wolf, Y., Mildner, A., Varol, D., Breker, M., Strauss-Ayali, D.,
1071 Viukov, S., Guilliams, M., Misharin, A., et al. (2013). Fate mapping reveals origins and
1072 dynamics of monocytes and tissue macrophages under homeostasis. Immunity *38*, 79–91.

1073 Zeisel, A., Muñoz-Manchado, A.B., Codeluppi, S., Lönnerberg, P., La Manno, G., Juréus, A.,
1074 Marques, S., Munguba, H., He, L., Betsholtz, C., et al. (2015). Brain structure. Cell types in
1075 the mouse cortex and hippocampus revealed by single-cell RNA-seq. Science *347*, 1138–
1076 1142.

1077 Xu, W., Hiếu, T., Malarkannan, S., and Wang, L. (2018). The structure, expression, and
1078 multifaceted role of immune-checkpoint protein VISTA as a critical regulator of anti-tumor
1079 immunity, autoimmunity, and inflammation. Cellular & Molecular Immunology 2017 15:5
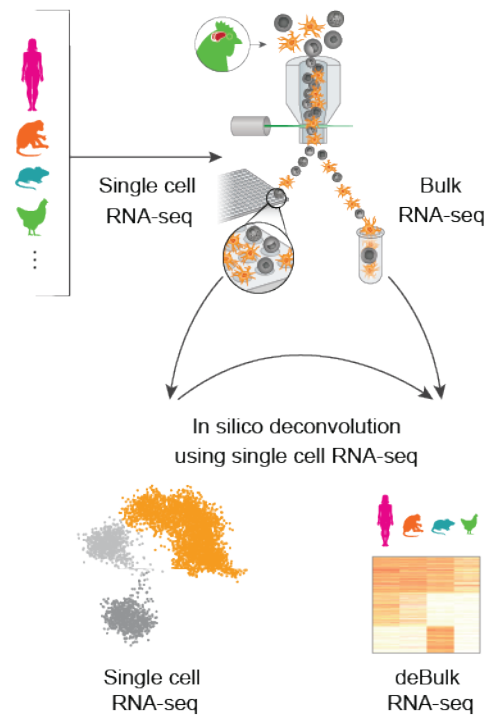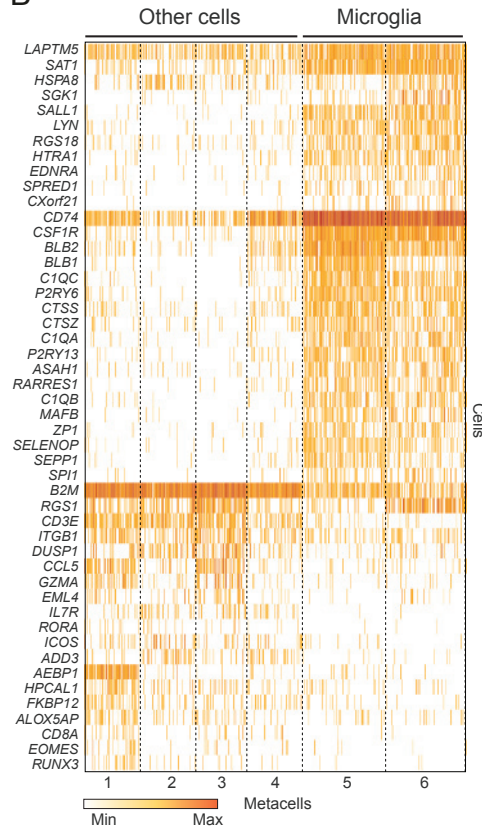1080 *15*, 438–446.

Figure 1

Click here to access/download;Figure;Figure 1.pdf ⬇

Figure 1 - Geirsdottir et al.,

Figure 2

Click here to access/download;Figure;Figure 2.pdf ⬇
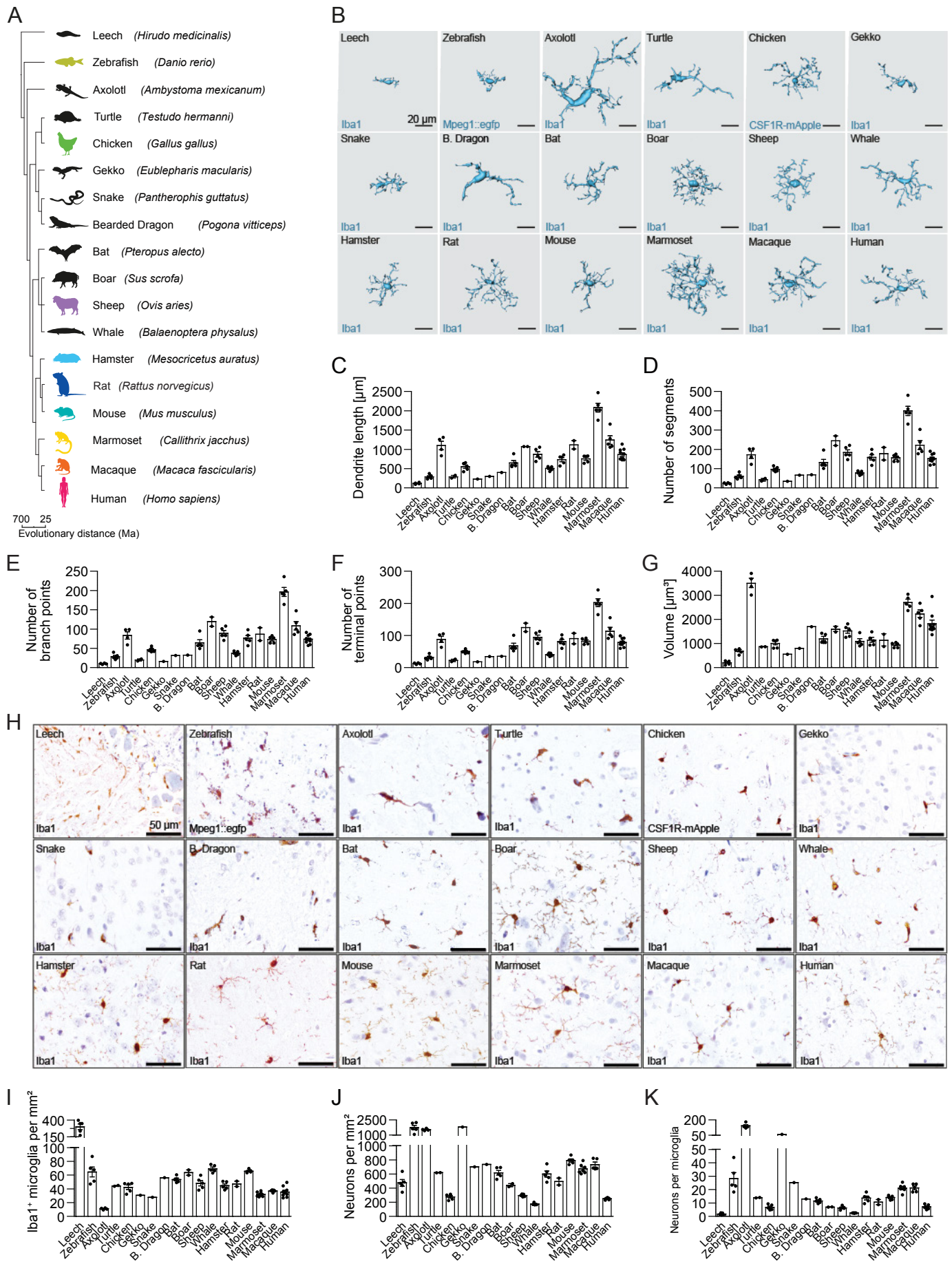
Figure 2 - Geirsdottir et al.,

Figure 3

Click here to access/download;Figure;Figure 3.pdf ⬇
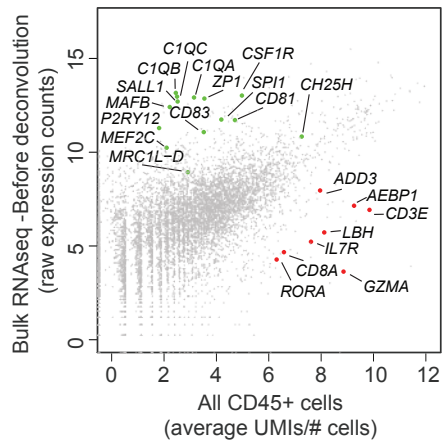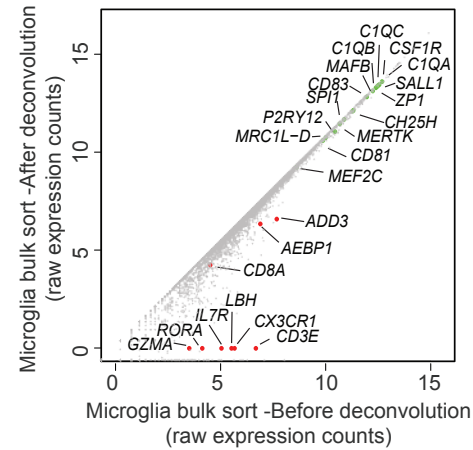
Figure 3 Geirsdottir *et al.*,
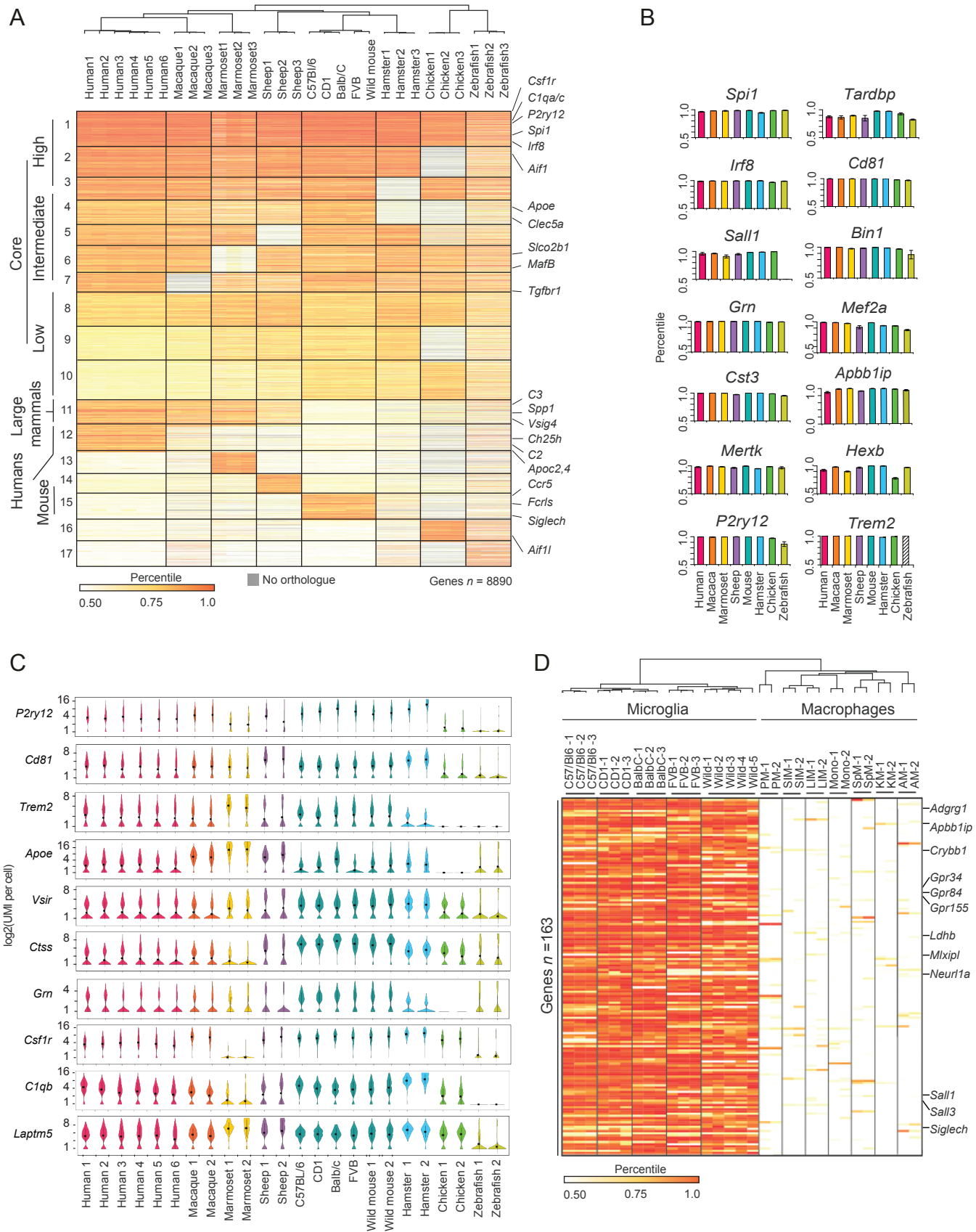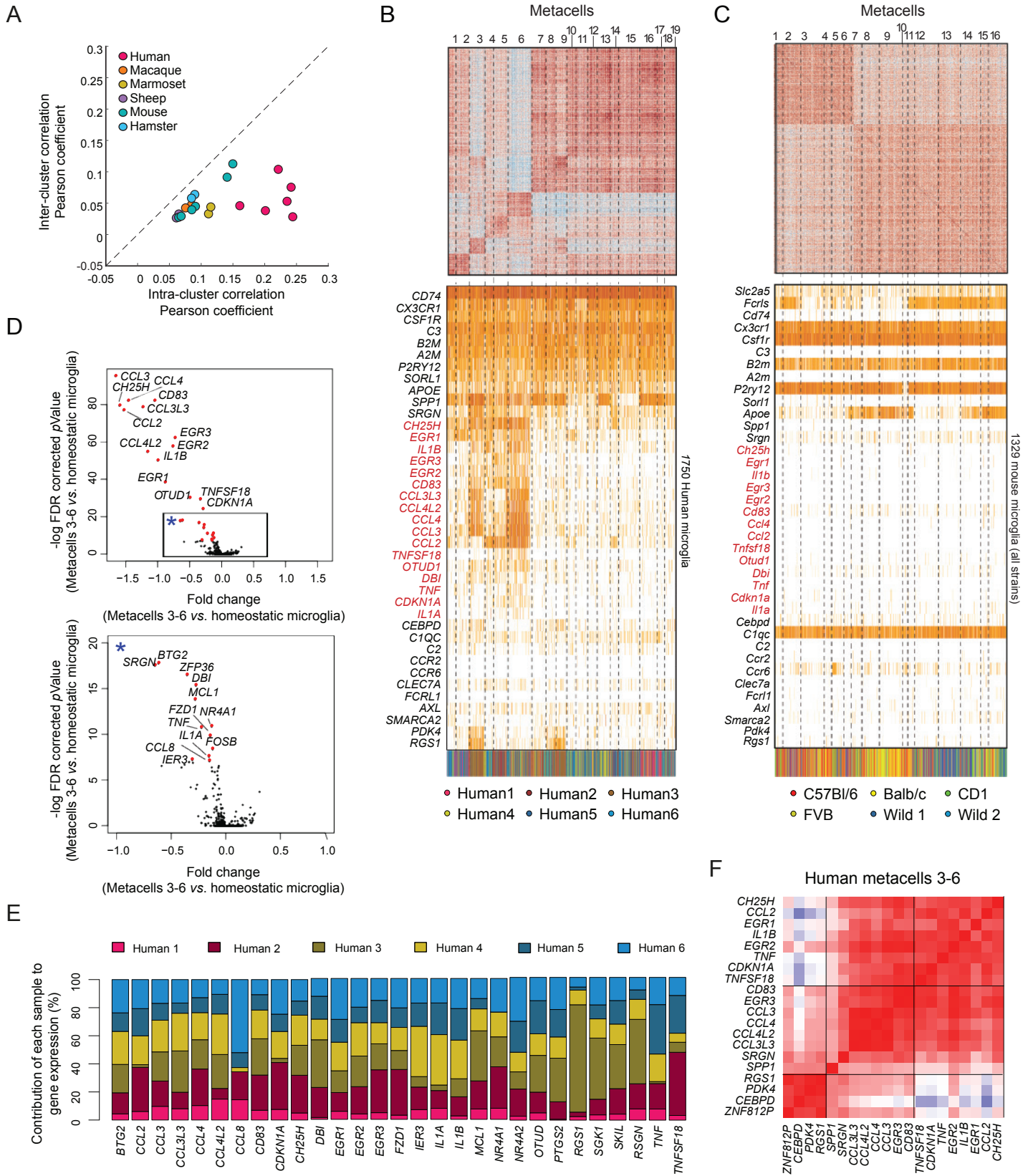
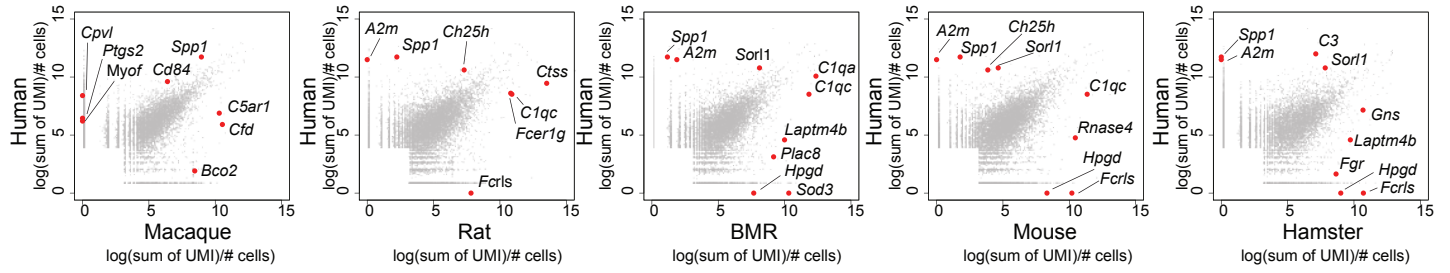Figure 4

Click here to access/download;Figure;Figure 4.pdf ⬇
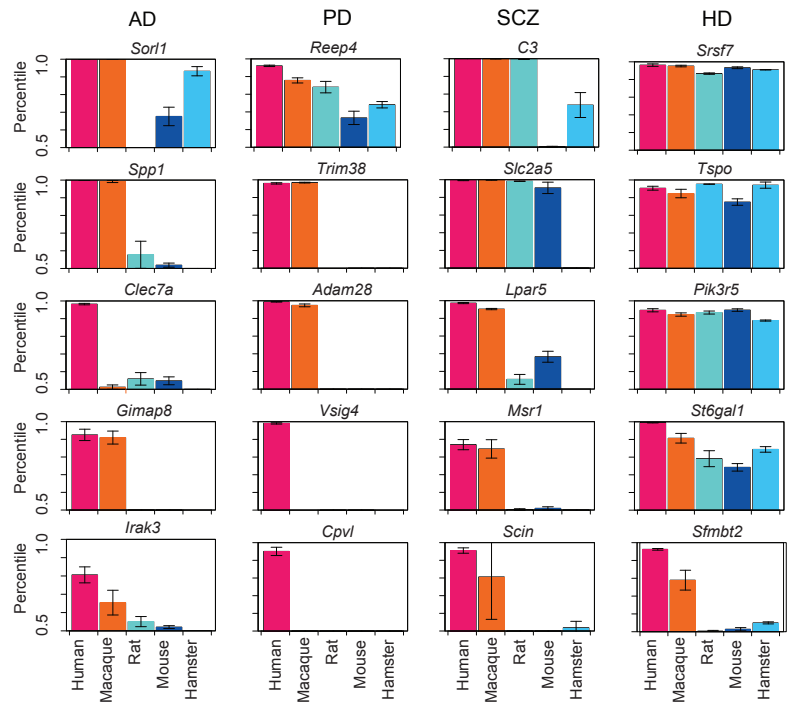
Figure 4 Geirsdottir *et al.,*

Figure 5 Geirsdottir et al.,
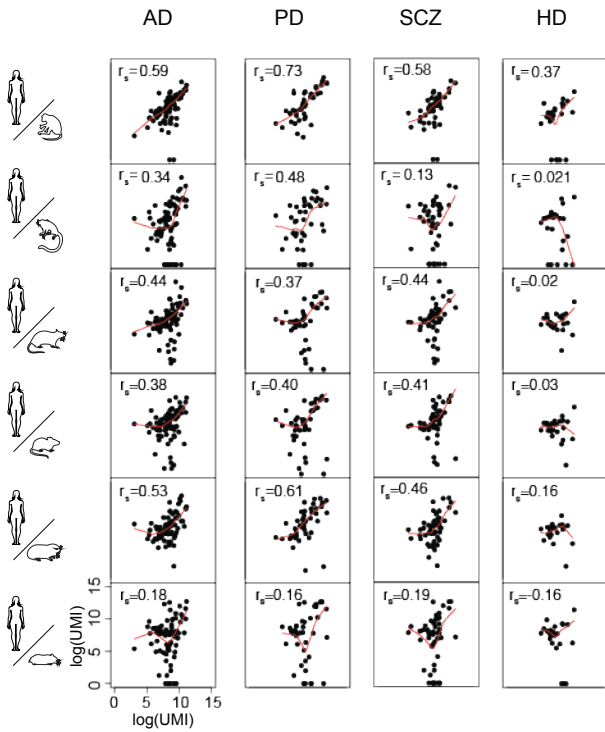
KEY RESOURCES TABLE

REAGENT or RESOURCE	SOURCE	IDENTIFIER
Antibodies		
CD45-PE, non-human primate	Miltenyi Biotec	250204
Mouse anti-chicken CD45 APC	Southern Biotech	8270-11
Mouse anti-pig CD45 FITC	Bio-Rad	MCA1222F
anti-human CD45	BioLegend	304008
Marmoset CD45 PE	BioLegend	250204
Anti-mouse/human CD11b	eBioscences	17-0112-83
Goat polyclonal CD11b antibody	Abcam	Ab62817
Iba-1	Wako	019-19741
Anti-leech Iba1	Jacopo Vizioli	Drago et al., 2014
anti-GFP	Invitrogen	A11122
anti-mCherry	Abcam	ab125096
Alexa Fluor 568	Life technologies	A11011
anti-P2Y12	AnaSpec	AS-55043
anti-Pu.1	Cell Signaling	2258S
anti-Pu.1	Abcam	ab209983
Hu FcR Binding blocker	eBiosciences	14-9161-73
Mouse FcR blocking antibody	BD Biosciences	553141
Chemicals, Peptides, and Recombinant Proteins		
Zombie Fixable Viability Kit	BioLegend	423101
Percoll	Sigma	P1644
1xPBS	Sigma	D8537
10xPBS	Gibco	70013065
HBSS	Gibco	14170112
HEPES	Gibco	15630056
Glucose 45 %	Sigma	G8769
Deposited Data		
Lavin, Y., Winter, D., Blecher-Gonen, R., David, E., Keren-Shaul, H., Merad, M., Jung, S., and Amit, I. (2014). Tissue-resident macrophage enhancer landscapes are shaped by the local microenvironment. Cell *159*, 1312–1326.	GSE63341	DOI.10.1016/j.cell.2014.11.018
Experimental Models: Organisms/Strains		
C57BL/6NCrl	Charles River-Germany	
BALB/cAnNCrl	Charles River-Germany	
Crl:CD1(ICR)	Charles River-Germany	
FVB	Charles River-Germany	

Wild Mouse /France	Diethart Tautz: Max-Planck-Institute Plön	
RjHan:AURA	Janvier Laboratory-Germany	
Zebrafish mpeg1:EGFP	Francesca Peri, EMBL Heidelberg	
Callithrix jacchus	Christine Stadelmann, Neuropathology, Göttingen	
Ovis Aries	Stephan Meckel, Neuroradiology, Uniklinikum Freiburg	
Gallus gallus CSF1R-mApple	Adam Balic, Roslin Institute	
Eublepharis macularis	Pet shop	
Panterophis guttatus	Pet shop	
Balaenoptera physalus	Lífvísindasetur Læknagarðs, Iceland	
Pteropus alecto	Florent Ginhoux, A*STAR Singapore	
Ambystoma mexicanum	Pet shop	
Hirudo medicinalis	Jacopo Vizioli, University Lille	
Testudo hermanni	Kaspar Matiasek	
Pogona vitticeps	Kaspar Matiasek	
Sus scrofa	local hunter	
Rattus norvegicus	Tali Kimchi	
Spalax ehrenbergi	Tali Kimchi	
Software and Algorithms		
MATLAB R2017b	MathWorks	http://www.mathworks.com/
R 3.5.0	The R Foundation	http://www.r-project.org/
Hisat 0.1.6	Kim et al., 2015	http://www.ccb.jhu.edu/software/hisat/index.shtml
GENE-E version 3.0.215	Copyright 2013 Broad Institute, Inc.	https://software.broadinstitute.org/GENE-E/
FlowJo software	FlowJo, LLC	https://www.flowjo.com
IMARIS software	Bitplane	http://www.bitplane.com/
Other		
MARS-seq reagents	(2014). Massively parallel single-	DOI. 10.1126/science.1247651

	cell RNA-seq for marker-free decomposition of tissues into cell types. *343*, 776–779.	

Figure S1 - Related to Figure 1

Figure S2

Figure S2 - Related to Figure 1

A Cortex (Frontal cortex)
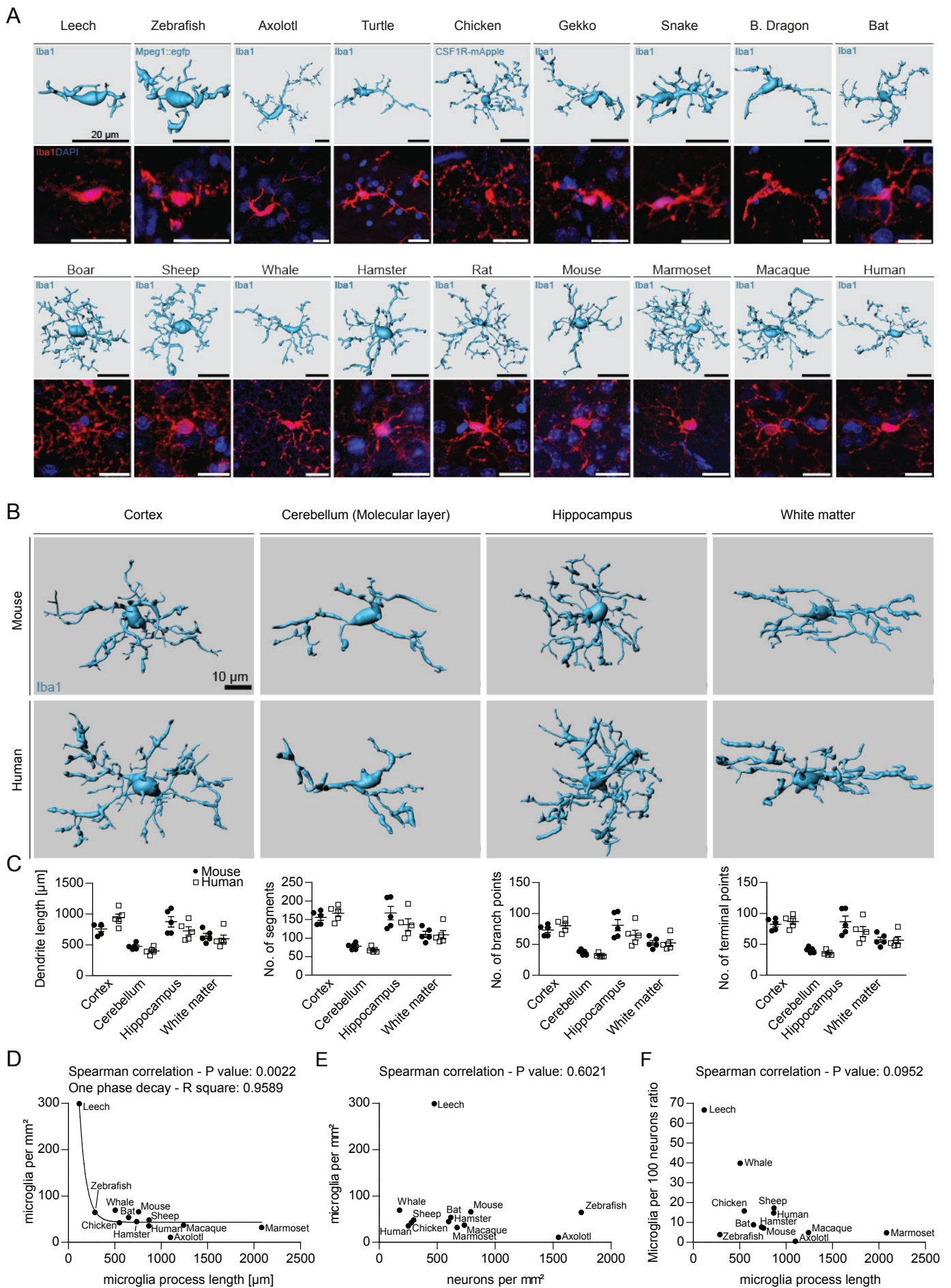
B Cerebellum (Molecular layer)
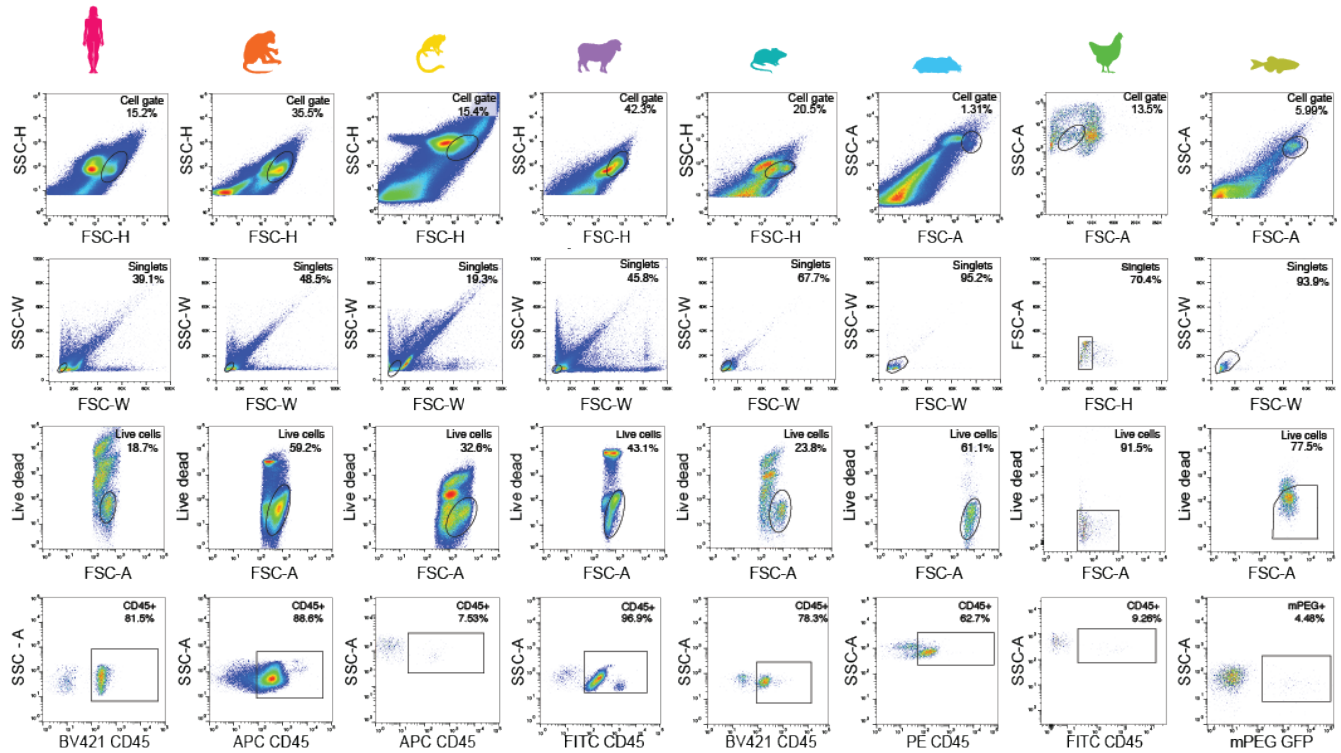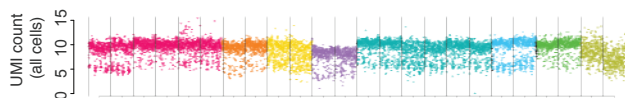
C Hippocampus (Dentate gyrus)

D White matter

Figure S3 - Related to Figure 2

A

B

C

D

E

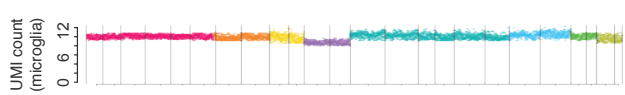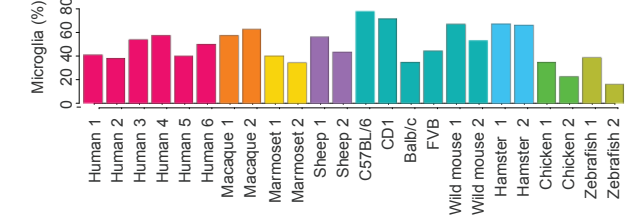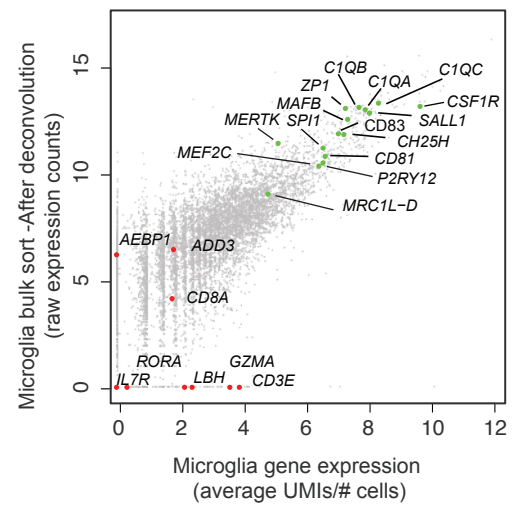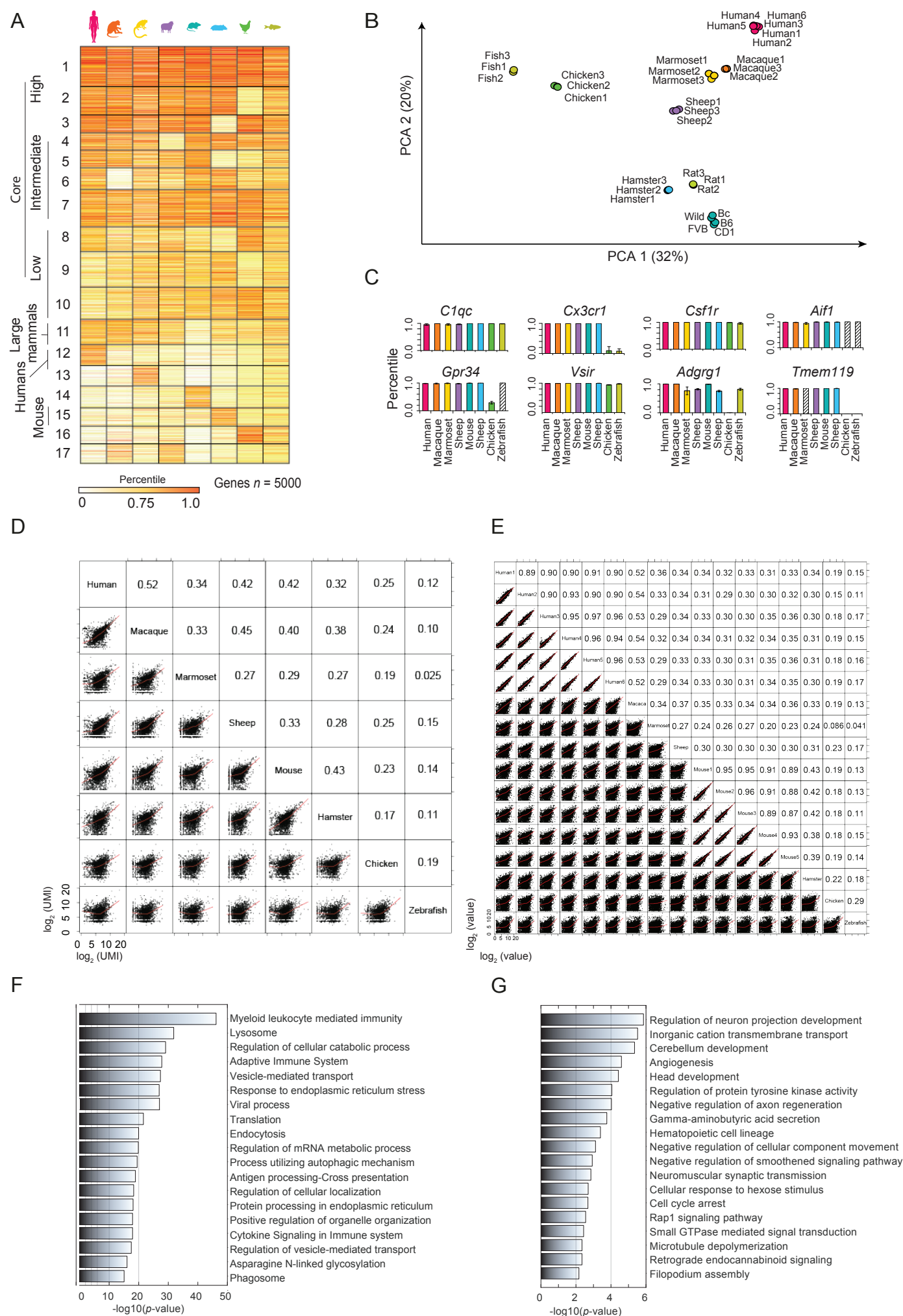# Figure S4 - Related to Figure 3

Figure S5 -Related to Figure 3

A

B

Figure S6 - Related to Figure 4

A — Metacells — 284 Marmoset microglia

C1QB, C1QC, TREML1, GAL, MARCKS, CX3CR1, B2M, ITM2B, TYROBP, TIMP2, VTN, APOE, CALCA, CST3, CST5, PAM, SERPINA1, TREM2, LAPTM5, P2RY12, TXNIP, P2RY13, IGSF1, C3, SORL1

B — Metacells — 458 Macaque microglia

CD74, CX3CR1, CSF1R, C3, B2M, A2M, P2RY12, SORL1, APOE, SPP1, SRGN, EGR1, IL1B, EGR2, CD83, CCL4L4 / CCL3L3, CCL4, CCL2, CEBPD, PDK4, RGS1, C1QC, CCR2, CCR6, CLEC7A, FCRL1, AXL, TNLG2A, OTUD1, DBI, TNF, CDKN1A, IL1A, SMARCA2

C — Metacells — 510 Hamster microglia

Cx3cr1, Csf1r, C3, B2M, P2ry12, Apoe, Cd83, Cebpd, Rgs1, Cd74

D — Metacells — 381 Sheep microglia

CD74, CX3CR1, CSF1R, B2M, A2M, P2RY12, SORL1, APOE, C1QC, AXL

E — Metacells — 455 Wild mouse microglia

Cd74, Cx3cr1, Csf1r, C3, B2m, A2m, P2ry12, Sorl1, Apoe, Spp1, Srgn, Ch25h, Egr1, Il1b, Egr3, Egr2, Cd83, Ccl4, Ccl2, Cebpd, Pdk4, Rgs1, C1qc, C2, Ccr2, Ccr6, Clec7a, Fcrl1, Axl, Tnfsf18, Otud1, Dbi, Tnf, Cdkn1a, Il1a, Smarca2

F
- C57BL/6
- CD1
- Balb/c
- FVB
- Wild

G
Apoe, Ccr6, Fcrls, Slc2a5

H
Wild mouse - Raw bulk expression (log) vs SPF mouse - Averaged raw bulk expression (log)

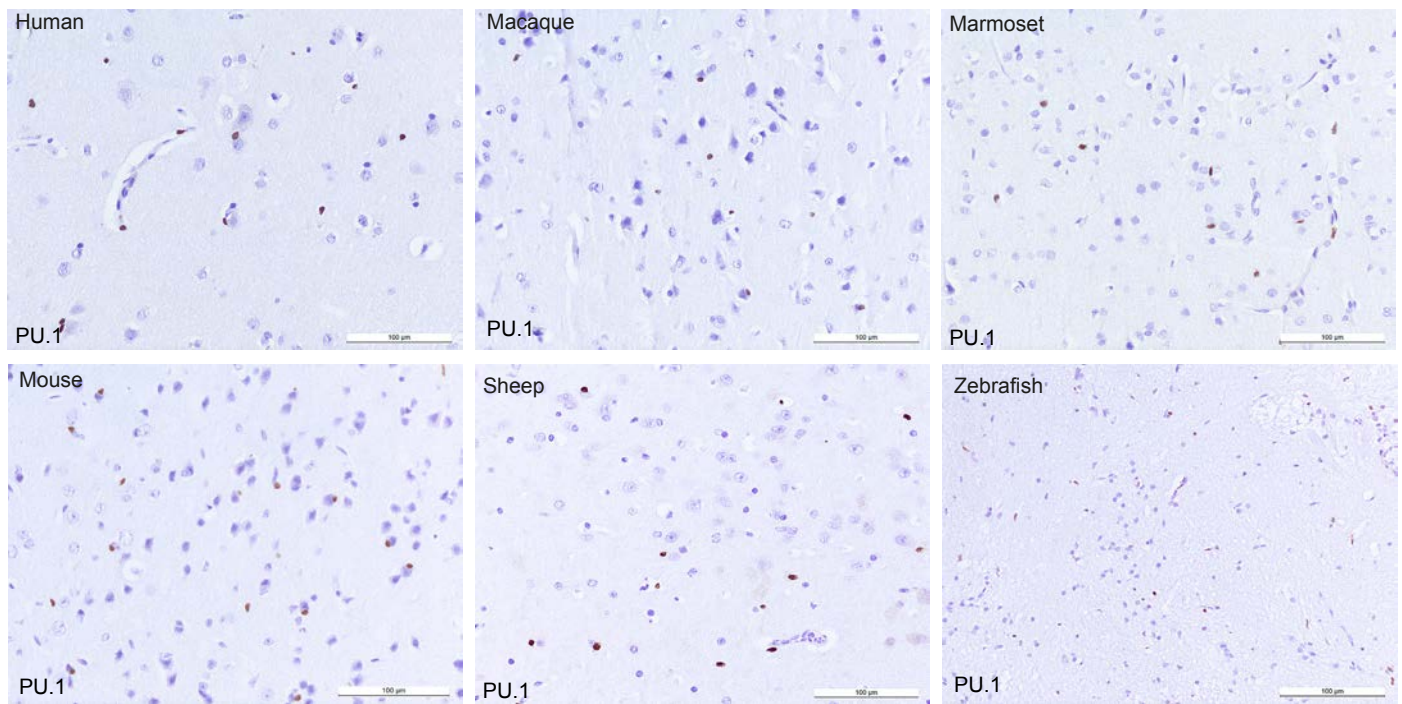Arhgef28, Sapcd1, St8sia6, Ddit4, Nudt7, Ildr2, Itgae, Klf4, Ly6e, Ctc1, Scoc, Tmem44, Izumo4, Rgs7bp, P3h2
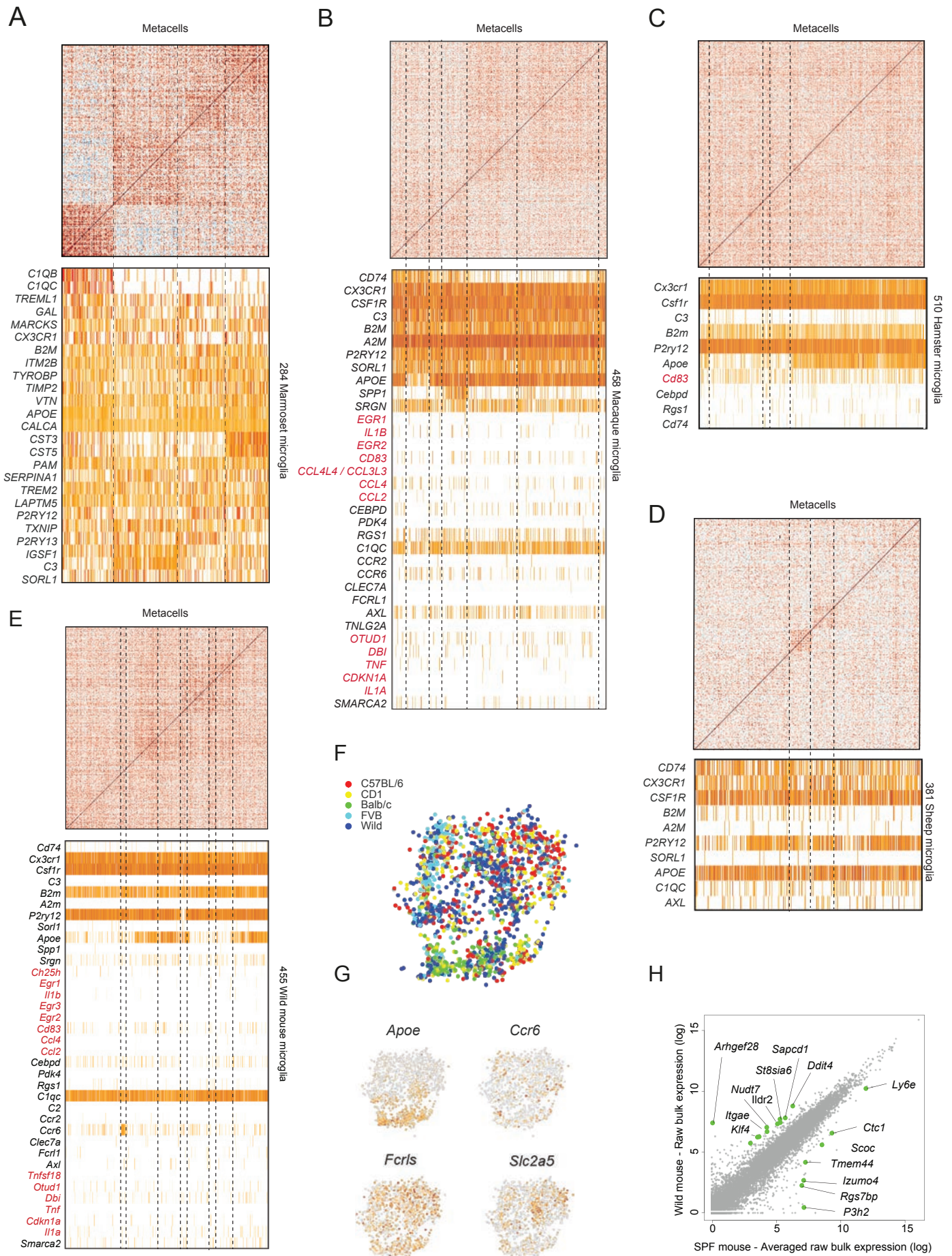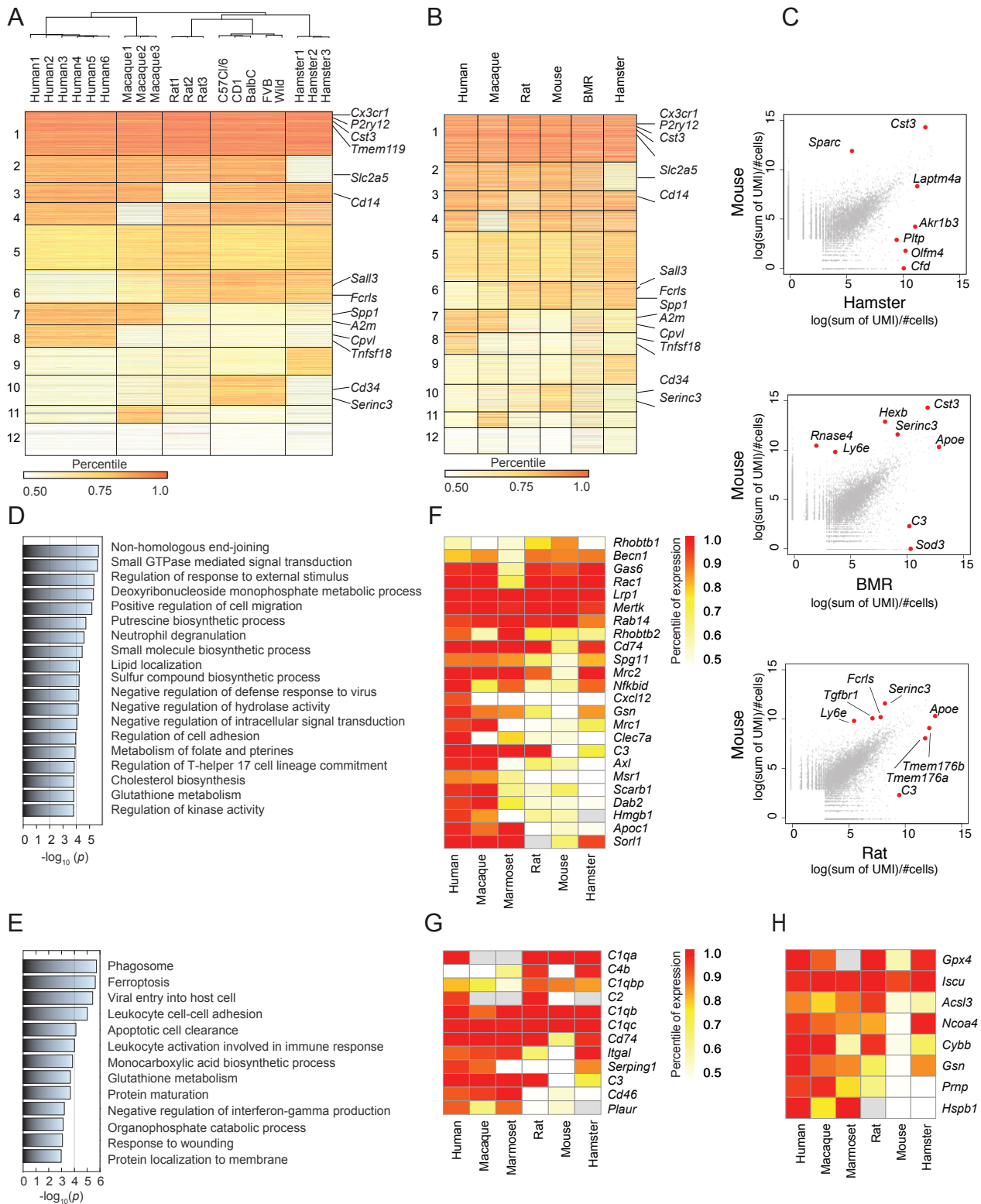
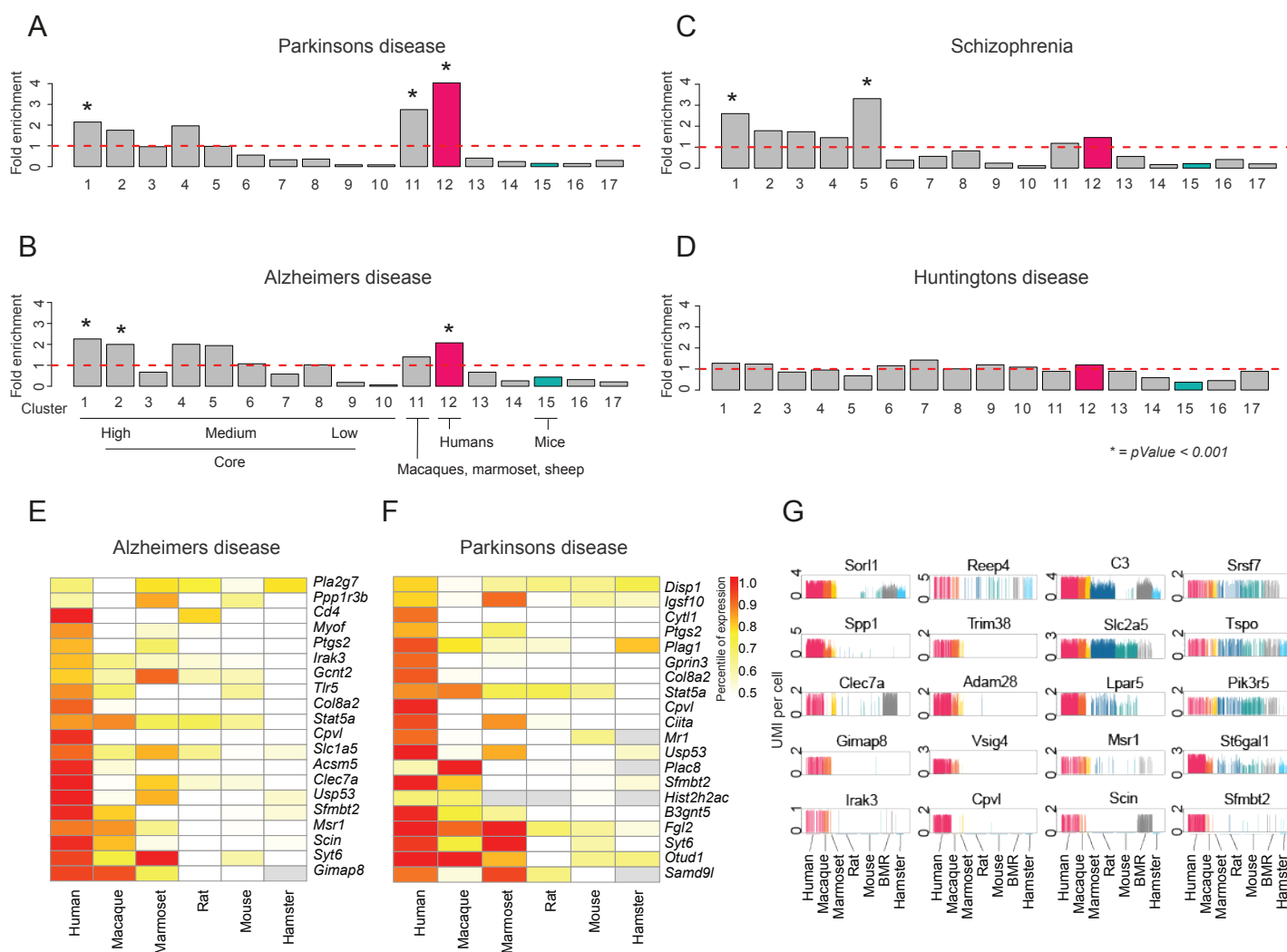# Figure S7 - related to Figure 5

Figure S8 - related to Figure 5

Click here to access/download
ZIP File
Table S1.xlsx

Table S2

Click here to access/download
ZIP File
Table S2.zip

Table S3

Click here to access/download
ZIP File
Table S3.zip

Table S4

Click here to access/download
ZIP File
Table S4.zip

Table S5

Click here to access/download
ZIP File
Table S5.zip

Table S6

Click here to access/download
ZIP File
Table S6.zip